Carroll Rosemary (Orcid ID: 0000-0002-9302-8074)

Check for updates

Factors Controlling Seasonal Groundwater and Solute Flux from Snow-Dominated Basins

Rosemary W.H. Carroll[a,b], Lindsay A. Bearup[c], Wendy Brown[b], Wenming Dong[d], Markus Bill[d], and Kenneth H. Willlams[b,d]

[a]Desert Research Institute, Reno, NV 89512, USA
[b]Rocky Mountain Biological Laboratory, Gothic, CO 81224, USA
[c] Lawrence Berkeley National Laboratory, Berkeley, CA, USA*
[d]Lawrence Berkeley National Laboratory, Berkeley, CA, USA

*currently at the United States Bureau of Reclamation, Lakewood, CO, USA

Correspondence to: Rosemary W.H. Carroll (Rosemary.Carroll@dri.edu), Division of Hydrologic Sciences, Desert Research Institute, 2215 Raggio Parkway, Reno, NV 89512

Running Head: Seasonal Groundwater and Solute Flux

Author Manuscript

This is the author manuscript accepted for publication and has undergone full peer review but has not been through the copyediting, typesetting, pagination and proofreading process, which may lead to differences between this version and the Version of Record. Please cite this article as doi: 10.1002/hyp.13151

This article is protected by copyright. All rights reserved.

Author Manuscript

Abstract. Critical zone influences on hydrologic partitioning, subsurface flow paths and reactions along these flow paths dictate the timing and magnitude of groundwater and solute flux to streams. To isolate first-order controls on seasonal streamflow generation within highly heterogeneous, snow-dominated basins of the Colorado River, we employ a multivariate statistical approach of end-member mixing analysis (EMMA) using a suite of daily chemical and isotopic observations. Mixing models are developed across 11 nested basins (0.4 km^2 to 85 km^2) spanning a gradient of climatological, physical and geological characteristics. Hydrograph separation using rain, snow and groundwater as end-members indicates that seasonal contributions of groundwater to streams is significant. Mean annual groundwater flux ranges from 12% to 33% while maximum groundwater contributions of 17% to 50% occur during baseflow. The direct relationship between snow water equivalent (SWE) and groundwater flux to streams is scale dependent with a trend toward self-similarity when basins exceed 5.5 km^2. We find groundwater recharge increases in basins of high relief and within the upper sub-alpine where maximum snow accumulation is coincident with reduced conifer cover and lower canopy densities. The mixing model developed for the furthest downstream site did not transfer to upstream basins. The resulting error in predicted stream concentrations points toward weathering reactions as a function of source rock and seasonal shifts in flow path. Additionally, the potential for microbial sulfate reduction in floodplain sediments along a low gradient, meandering portion of the river is sufficient to modify hillslope contributions and alter mixing ratios in the analysis. Soil flushing in response to snowmelt is not included as an end-member but is identified as an important

This article is protected by copyright. All rights reserved.

Author Manuscript

mechanism for release of solutes from these mountainous watersheds. EMMA used in combination with high frequency observations reveals important aspects of catchment hydrodynamics across scale.

Keywords: Colorado River; mountainous watershed; snow; end-member mixing analysis; groundwater

1 Introduction

Snow-dominated systems provide water for one-sixth of the world's population, are considered especially vulnerable to climate change (IPCC, 2014; MRI, 2015) and globally are experiencing large-scale tree mortality (Allen et al., 2010; Anderegg et al., 2012). Climate induced modifications to snow accumulation, melt and subsequent water budget partitioning is expected to decrease stream flow (Clow, 2010; Vano et al., 2012; Edburg et al., 2012; Hoerling et al., 2013; Lukas et al., 2014; Barnhart et al., 2016; Li et al., 2017; McCabe et al., 2017) and potentially alter hydrologically mediated biogeochemical processes that control solute sourcing and transport from these systems (Maher, 2011; Perdrial et al., 2014; Winchell et al., 2016; Krause et al., 2017). Watersheds more dependent on groundwater could be buffered against climate extremes to enhance resilience for downstream water and environmental management (Taylor et al., 2012). However, uncertainty exists regarding the role of groundwater contribution to snow-dominated, low-order streams residing in basins of large relief. If hydraulic gradients approximate topography, steeper watersheds would result in shorter travel times and promote

This article is protected by copyright. All rights reserved.

Author Manuscript

greater dependence on processes of surface runoff and interflow (Beven and Kierby, 1979; Tetzlaff et al., 2009). However, watersheds with apparently low storage contain "long memory" of past inputs (Kirchner, 2003) as supported by chemostatic behaviour (Godsey et al., 2009). Our conceptual understanding of hydrologic partitioning to either runoff or recharge is complicated in these mountainous systems by the difficulty of quantifying snow distribution and melt at the watershed scale (Dietermann and Weiler, 2013; Kormos et al., 2014) along with the tight coupling of vegetation structure to climate and topography, and its influence on spatial and temporal energy and water budget components (Bearup et al., 2014; Godsey et al., 2014; Biederman et al., 2015; Carroll et al., 2017).

Hydrologic and geochemical observations can quantify the routing of water from the surface and subsurface to streams. Filter-based approaches solely dependent on stream flow (Nathan and McMahon, 1990; Arnold et al., 1995) have been used to identify groundwater contributions to streams across a range of scales from small catchments (Wilcox and Huang, 2010) to regional (Santhi et al., 2008) and global assessment (Beck et al., 2013). However, chemical mass balance approaches that incorporate stream concentration-discharge (C-Q) relationships represent an integrated hydrologic response of the individual catchment with a direct link to contributing sources, associated flow paths, and groundwater residence times (Kirchner, 2009) and have been a valuable method in studying energy, water and solute fluxes across the critical zone (CZ) – defined from bedrock to canopy. Brooks et al. (2015) stresses C-Q patterns that incorporate tracers of differing sources and mobility can improve understanding of how water and solutes are stored and

This article is protected by copyright. All rights reserved.

transported through a watershed. Conservative tracers, such as the stable isotopes δ^2H and $\delta^{18}O$, provide information on water movement, while solutes such as Ca, Mg, Na and Si reflect weathering process. Metals and non-conservative trace elements can parse out redox controls on weathering and biogeochemical processes. As such, C-Q observations have been used to quantify the timing and source of groundwater recharge (Bearup et al., 2014), vertical weathering gradients and subsurface flow paths (Winnick et al., 2017), lithologic and vegetation controls on solute export (Wymore et al., 2017), and reaction-rate kinetics (Maher, 2011). C-Q observations can thereby identify conceptual and predictive models of hydrologic partitioning, routing and stream export with greater certitude of getting the "right answer for the right reasons" (Kirchner, 2006; Brooks et al., 2015).

To better understand source contributions influencing the timing of water and solute export, we employ a multivariate, statistical approach (Hooper, 2003) of end-member mixing analysis (EMMA) using a suite of natural chemical and isotopic observations. EMMA is applied across 11 snow-dominated, nested basins ranging from 0.4 km^2 to 85 km^2 to investigate first-order topographic, geologic and vegetation controls of groundwater and solute flux to streams. Additionally, we superimpose the mixing model developed for the furthest downstream and most heavily characterized stream gauge in the study site onto all contributing basins. The mixing space scales if the seasonal ratios among solutes are maintained. In contrast, lack of a common mixing space occurs if water originates with a different chemical signature, or experiences dissimilar hydrologic partitioning to influence flow path and subsequent exchanges along this

Author Manuscript

This article is protected by copyright. All rights reserved.

flow path. In this manner, EMMA provides insight to CZ feedbacks as reflected in C-Q behavior for hydrodynamic conceptual model development of water and tracer movement.

2 Site Description

The East River (ER) is a snow-dominated, headwater basin of the Upper Colorado River Basin (UCRB) located in the western United States (US) (Figure 1). The ER is the designated testbed of Lawrence Berkeley National Laboratory's Watershed Function Scientific Focus Area (WFSFA). Through WFSFA, observational networks have been established to measure stream discharge and precipitation chemistry. The ER is considered representative of many snow-dominated headwaters of the Rocky Mountains (Battaglin et al., 2011; Markstrom et al., 2012). The study domain encompasses nearly 85 km^2, a 1.4 km vertical drop in elevation (4120 m to 2760 m) and pristine alpine, sub-alpine, montane, and riparian ecosystems. The ER contains high-energy mountain streams to low-energy meandering floodplains and is eroding primarily into the Cretaceous, carbon-rich, marine shale of the Mancos Formation (Km, Figure 2). This shale is ubiquitous throughout the UCRB and is characterized by poor groundwater quality with high concentrations of dissolved solids, SO_4, heavy metals, and nutrients (Apodaca, 1997). The ER geology has distinct lithologic differences moving west to east (Figure 2). Cenozoic igneous formations have intruded into the Mancos Formation along the western edge of the study domain and into Paleozoic and Mesozoic sedimentary strata along the east where it forms steeply dipping beds and surface exposure of older units (Gaskill et al., 1991).

Author Manuscript

This article is protected by copyright. All rights reserved.

Author Manuscript

Climate for the area is defined as continental subarctic with long, cold winters and short, cool summers. Two snow-telemetry (SNOTEL) sites occur in the vicinity of the ER domain: Schofield (Site Number: 737) and Butte (Site Number: 380) at elevations 3261 m and 3097 m, respectively. Snowfall occurs October through May, while monsoonal rains generally begin in mid-July and last into September. Mean daily air temperatures at Butte range from -8.3°C in December to 11°C in June, with an average decrease of 1.6 ± 1.2°C at the higher elevation Schofield station, although inversions of 1°C in maximum daily air temperature occur consistently between the SNOTEL sites from October to February. Annual precipitation for the 30-year period of record at Schofield is 1200 ± 233 mm yr^{-1} with approximately 70 ± 8% falling as snow. On average, Butte total precipitation is approximately half of Schofield at 670 ± 120 mm yr^{-1} with snow accounting for 66 ± 12% annual precipitation. Our study focuses on water year 2016 which represents slightly less than average precipitation. In 2016 Schofield experienced 970 mm total precipitation with snowfall at 60%; while Butte was 690 mm of which 51% was snow. Figure 3 shows 2016 peak SWE at Schofield occurred on May 2 (698 mm), while Butte peak SWE occurred April 2 at half the accumulation (335 mm) and became snow-free three weeks prior to the Schofield station on May 25.

The Pumphouse C-Q station (Basin ID = 11; Figure 1) represents the furthest downstream monitoring station and has the highest resolved stream chemistry (daily). Discharge (Figure 3) is dominated by snowmelt processes with flow peaking in early June at 12 m^3 s^{-1} in response to high elevation snowmelt, but only after several initial subsidiary rises in the

This article is protected by copyright. All rights reserved.

hydrograph driven by snowmelt at lower elevations as exemplified by Butte. After peak discharge, flow recedes through the summer and fall with monsoonal storm events occurring in late summer causing small, transient increases in discharge. Baseflow occurs in the fall and winter months. Ten basins are located in the upper portions of the watershed with stream chemistry collected weekly to monthly at C-Q locations (Figure 1). Physical attributes of all basins are provided in Table 1 with discharge characteristics given in Table 2 and detailed hydrographs presented in Figure S10. Basins 2-9 are tributaries while East above Quigley (EAQ; ID = 1), East below Copper (EBC; ID = 10) and Pumphouse reside along the ER main stem.

We classify existing vegetation type (Figure 4) using United States Geological Survey (USGS) Landfire 30-m raster maps (Landfire, 2008) and consolidated by dominant life-form (Table S1). The ER is predominantly barren and sparsely vegetated land cover of alpine conditions (26%) and conifer forests (45%). Conifer forests are classified as Rocky Mountain subalpine dry-mesic Spruce-Fir forest (97%), with only minor representation of Rocky Mountain Lodgepole Pine. Aspen forests occupy 12% of the basin's area while grasslands (10%), shrubs (2%), riparian (3%), and other (developed and open water, 2%) represent the remaining land cover. Figure 5 (and Figure S3) illustrates dominate land cover by elevation. Aspen occur only at elevations less than 3500 m. Conifer species outcompete aspen at elevations above 3100 m, while barren conditions dominate at 3650 m, and are the sole classification at elevations exceeding 4000 m. Lower tree cover density is biased toward higher elevations (Figure 5d) and

Author Manuscript

This article is protected by copyright. All rights reserved.

along southern and southwestern aspects, while denser forests occupy aspects toward the north and northeast (Figure S6b).

3 Methods

3.1 Solute Collection and Chemical Analysis

Geochemical analysis of all water samples includes δ^2H and $\delta^{18}O$, cations and trace metals, anions as well as dissolved non-purgeable organic carbon (NPOC) and dissolved inorganic carbon (DIC). Filtered samples (Pall, NY, USA; PTFE; 0.45 μm) were collected *in situ* at all C-Q locations except for Pumphouse stream water samples that were collected daily using an automatic water sampler (Model 3700; Teledyne ISCO, NE, USA) via a peristaltic pump and uncapped 1 L polyethylene bottles. A separate ISCO sampler was established for stable isotopes with each bottle filled with 2 cm mineral oil to eliminate evaporation effects between collection and retrieval of samples.

Stable isotope samples were placed in 1.5 mL glass vials with Teflon™ coated septa lids. Hydrogen and oxygen isotope ratios of water were measured using an Off-Axis Integrated Cavity Output Spectrometer coupled to an auto-sampler interfaced with a heated injector block (Los Gatos Research, San Jose, USA). Hydrogen and oxygen isotope ratios are reported in conventional δ-notation relative to Vienna Standard Mean Ocean Water scale. Anion samples were stored in high-density polyethlene vials with Cl, NO_3, and SO_4 measured using an ion chromatograph (ICS-2100, Dionex, CA, USA) equipped with AS-18 analytical and guard

Author Manuscript

This article is protected by copyright. All rights reserved.

columns. Cation samples were preserved with trace metal grade 12 N HNO_3 and analyzed using ion coupled plasma mass spectrometry (ICP-MS) (Element 2, Thermo Fisher, MA, USA). Carbon samples were stored in no head-space 40 mL glass vials with NPOC concentrations determined as the difference between total dissolved carbon and DIC, with all measurements performed using a TOC-LCPN instrument (Shimadzu, MD, USA).

3.2 Rain Chemistry

In conjunction with grab samples to establish the local meteorological water line (LMWL, Figure S18), weekly aggregated rain samples (n=41) were collected to assess spatial variability in precipitation. Rain gauges made to US Weather Bureau specifications with a capacity of 27.9 cm x 2 mm were installed at four locations (Figure 1). Gauges were situated in areas sheltered from winds, attempting to maintain at least two lengths of surrounding tree height to avoid turbulence. Mineral oil was used to limit evaporative effects. Despite diverse locations in the watershed, and large variation in topographic relief, all four gauges exhibited similar isotopic values for the sampling period and experienced similar depletion during the summer and into the fall. An additional gauge was installed near the sampling location for the LMWL with no mineral oil to assess rain anions, cations, and trace metals. Data gaps were filled using weekly samples from the National Atmospheric Deposition Program (NADP) site CO10 located in Gothic, Colorado in the vicinity of C-Q site ID 9 (Figure 1).

Author Manuscript

This article is protected by copyright. All rights reserved.

Author Manuscript

3.3 Snow and Snowmelt

Snow depth at 3 m resolution (Figure S7) was obtained from NASA's LiDAR-based Airborne Snow Observatory (ASO) flown over the ER on April 4-6, 2016 at approximately peak SWE (Figure 3). ASO uses a Riegl Q1560 airborne laser scanner to perform geodetic mapping of snow depth by differencing snow-free and snow-covered elevation data sets. Painter et al. (2016) provides a full discussion on the technical, operational, and algorithm retrieval for snow depth. In conjunction with ASO, 13 snow pits were situated to the capture the broadest range in elevation (2728 m to 3620 m) with safe winter access (Figure 1). Snow pits were dug in open, flat areas with mass and isotopic composition measured at 10 cm intervals. Pit depths ranged from 67 cm to 140.5 cm, with total SWE (21.4 cm to 66.5 cm) correlated to elevation ($r^2 = 0.63$, $p = 0.001$). In contrast, pit snow density (0.28 g cm^{-3} to 0.35 g cm^{-3}) showed less trend with elevation ($r^2 = 0.08$, $p = 0.36$). Therefore, a mean density for all sites (0.32 ± 0.02 g cm^{-3}) was applied uniformly to ASO depths to calculate SWE distribution in the ER. Anions, cations, and trace metals from snow pits were aggregated upon collection. To quantify the evolution of snow to snowmelt, we deployed snowmelt collection devices (modified from Kormos, 2005) at four locations (Figure 1) coincident with snow pits. Beginning April 1 sample collection began and continued until full melt was achieved (n=24). The difference in snow pit and snowmelt means was 2.31‰ and 17.37‰ for $\delta^{18}O$ and $\delta^{2}H$, respectively (Figure S18). Snowmelt enrichment over the snowpack is consistent with previous studies in the Rocky Mountains of Colorado (Mast et al., 1995).

This article is protected by copyright. All rights reserved.

Author Manuscript

3.4 Deep and Shallow Groundwater

Deep groundwater is defined using chemistry from the Inouye well (Well, Figure 1) drilled to 60 m in Mancos shale streaked with sandstone. Water levels occur 10 to 15 m below ground surface (D. Inouye, written communication, September 2017). Samples were collected weekly from a spigot, allowing water to flow for several minutes prior to collection. Seasonally shallow groundwater is defined by ephemeral seeps emerging from the hillslope toe (May, n=3) and a mid-slope region (June, n=6) in the vicinity of the Pumphouse stream gauge. Lastly, four 10m wells along a hillslope transect adjacent to the Pumphouse stream gauge were sampled in November, 2016 (unsaturated n = 8; and saturated n = 12) to compare to the deep groundwater end-member.

3.5 Stream Discharge

Instantaneous stream discharge measurements using a SonTek Flow Tracker® acoustic Doppler velocimeter were made at all C-Q locations to create depth-discharge relationships in conjunction with Solinst Levellogger Edge® pressure transducers corrected with barometric pressure. Correlation of daily flows with the USGS stream gauge East River at Almont (site ID. 09112500) located approximately 25 km downstream from the study site allowed correction of stream discharge at Pumphouse during iced periods in the winter when pressure transducer readings are anomalously high (Melcher and Walker, 1992). EMMA was applied to seasonal hydrographic periods observed at each station. Specifically, the rising limb occurs as the first

This article is protected by copyright. All rights reserved.

major inflection of increased flow in early spring to peak discharge. The falling limb extends from peak discharge to the onset of the monsoons. In 2016, the monsoon period is defined as July 18 to the end of the water year determined from heavy rains measured at Butte SNOTEL. Baseflow occurs prior to the rising limb and after the monsoon rains.

3.6 Mixing Model and Hydrograph Separation

Hydrograph separation is based on the multivariate approach of EMMA (Hooper, 2003). A full review of mathematics is provided in section S.3.1. EMMA relies on principal component analysis and does not require explicit identification of end-members to define the lowest dimension (m) of the mixing sub-space. Principal components are retained if they explain more variance than the original variables with the additional constraint that the minimum dimension effectively removes patterns from the distribution of residuals between simulated and predicted stream concentrations. Appropriate end-members must be chemically distinct from each other and bound the stream concentrations in the projected eigenvector mixing space (U-space). Hydrograph separation is performed in U-space by solving m+1 system of linear equations to conserve mass. To illustrate, if m=2, then three end-members are needed,

$$U1 = f_1 U1_1 + f_2 U1_2 + f_3 U1_3 \quad (1a)$$

$$U2 = f_1 U2_1 + f_2 U2_2 + f_3 U2_3 \quad (1b)$$

$$1 = f_1 + f_2 + f_3 \quad (1c)$$

Where f_1, f_2, and f_3 are the streamflow fractions associated with end-members 1, 2 and 3, respectively, while U1 and U2 are the projections of each component. Temporal variation in

This article is protected by copyright. All rights reserved.

Author Manuscript

mixing follows methods presented by Bearup et al (2014) and done according to hydrographic characteristics.

Uncertainty associated with source contribution is done following methods similar to Cowie et al. (2017). The range in applicable tracer concentrations is calculated as the ±1 standard deviation (sd) about the seasonal mean (Figures S20-23). The seasonal mean is chosen to represent the central tendency of the dataset since outliers were removed at the onset of data analysis and all subsequent samples are considered meaningful. The influence of tracer variability is applied to U-space positioning and hydrograph separation. Specifically, tracers associated with each end-member are varied across their ±1sd range in observed concentrations while holding the other end-members at their mean value. The process is repeated for all end-members. Temporal uncertainty is estimated for each hydrograph period and reported as the minimum and maximum fractional contribution of each end-member based on all combinations of EMMA applied.

To allow a comparison of mechanisms controlling mixing across scales, we applied the mean EMMA developed at Pumphouse to the ten contributing areas located upstream. The error of the Pumphouse mixing model in replicating observed stream concentrations at each upstream location is calculated as prediction bias,

$$b_j = \sum_{i=1}^{n} \left(\hat{x}_{ij} - x_{ij}\right) \Big/ \bar{x}_j, \qquad (2)$$

with $\hat{x}_{ij}$ and x_{ij} the predicted and observed j^{th} solute concentration at time i, respectively; and $\bar{x}_j$ the average j^{th} solute concentrations over the evaluation period.

This article is protected by copyright. All rights reserved.

Author Manuscript

4 Results

4.1 Tracer Selection

Tracers are selected from the full suite of solutes sampled that exhibited near-linear behavior in bi-mixing plots of Pumphouse stream concentrations (Figure 6). Solute concentrations are at a minimum during spring runoff in June and at a maximum during baseflow. Deviations from linear behavior and exclusion of traditionally assumed tracers for EMMA, such as Cl, Na and K, are discussed in detail in section S.4.2. Different combinations of the identified solutes in Figure 6, along with δ^2H and $\delta^{18}O$, were run to find the model that described the greatest variance with the least number of dimensions while maintaining acceptable error in terms of residual trend analysis. The final model uses six solutes (Ca, U, Sr, SO_4, and stable isotopes) to describe 97% of the observed variance with m=2. SO_4, Ca, and $\delta^{18}O$ are the dominant predictors of model behavior. A review of EMMA model selection and variation in groundwater contributions to Pumphouse as a function of solute choice are provided in section S.3.2.

4.2 Seasonal Stream Source

A 2-dimensional model requires three end-members to solve Equation 1. Rain, snow, and deep groundwater chemistry plot distinctly in U-space and bound the Pumphouse stream chemistry (Figure 7) and are therefore appropriate. We assume a constant snow end-member based on the melt isotopic signature and the average of all available ion samples from snow pits,

This article is protected by copyright. All rights reserved.

Author Manuscript

melt and NADP winter samples. Weekly rain and groundwater chemistry are averaged for stream flow characteristics defining baseflow, rising, falling, and monsoon. Pumphouse baseflow chemically resides in the groundwater quadrant, then moves toward the snow signature during the rising limb and retracts toward groundwater during the falling limb. With monsoon rains, stream water moves closer toward the rain signature before settling back in the groundwater quadrant in the fall. Table 3 provides the resulting fractions of end-members in Pumphouse stream flow calculated for each of the hydrographic periods. Annually, the groundwater fraction contributing to stream waters (fGW) is 0.29 of the water at Pumphouse, with maximum fGW occurring during baseflow (0.43), and a minimum during the falling limb of snowmelt (0.18). The fraction of snow dominates most of the year (0.48 to 0.74). Snow contributions during periods of no snowmelt, such as baseflow, are reflective of subsurface water that has had insufficient time to react with host rock material along its flow path and thereby retains the snow signature. Rain comprises the smallest component of stream water (0.08 to 0.16) with this fraction at a maximum during the monsoon. EMMA was run independently for each of the ten basins contributing to Pumphouse using the solutes defined for the Pumphouse mixing model. Resulting fGW for individual basins is provided in Table 4. fGW are at a minimum during snowmelt runoff and at a maximum during baseflow for all basins. Gothic (Basin ID =6) has the lowest fGW for all seasons (0.07 to 0.17) while Copper Creek (Basin ID = 9) has the highest (0.17 to 0.50). The seasonal fractions of each end-member to stream flow are provided in Table S3 and plotted in Figure S24.

This article is protected by copyright. All rights reserved.

Author Manuscript

Estimated uncertainty in fGW across the different hydrographic periods for each sub-basin is provided in Table 4 and Figure S26. Uncertainty increases for end-members that plot closest to stream concentrations in U-space since a small change in end-member location can produce a relatively large change in contribution. During baseflow, stream concentrations reside closest to the groundwater end-member and uncertainty grows. During runoff, the influence of groundwater diminishes and uncertainty decreases. The range in fGW uncertainty grows as a function of mean fGW across all seasons ($p<<0.01$), though the slope defining this relationship changes. The slope is at a low during runoff (rising and falling, $m = 0.42$), increases during the monsoon ($m = 0.49$) and is at a high during baseflow ($m = 0.57$). To illustrate, Copper Creek has the largest estimated mean fGW across seasons and therefore it has the largest range in uncertainty. Specifically, Copper Creek's range in baseflow fGW is calculated as 0.39 to 0.68 (range 0.29) while the falling limb fGW is 0.14 to 0.22 (range 0.07). In contrast, Gothic Creek has the lowest estimated uncertainty in fGW with baseflow equal 0.13 to 0.23 (range 0.09) and during the runoff period equal to 0.06 to 0.09 (range 0.03). While we are focused on fGW, the influence of tracer variability with respect to other source contributions is discussed in detail in section S.5.1. Overall, the relative contributions of end-members remains proportionate across seasons, and using the mean tracer values for EMMA hydrograph separations is considered representative of relative source contributions within the ER basin.

Basin aggregated topographic, geologic, climatic, and vegetation characteristics (Table 1, refer to S.1) are investigated as first-order controls on fGW. Regressions with the greatest

This article is protected by copyright. All rights reserved.

Author Manuscript

explanatory power to mean annual predicted fGW are SWE, basin slope, basin relief, percent conifer, and tree cover density (Figure 8). In all cases, correlation and significance are greatly improved by excluding Avery or Marmot from the analysis. These small basins are difficult to delineate topographically, and channel instability as evidenced by a high number of avulsed channels across the exiting alluvial fan, suggest complex surface water and groundwater hydrology not fully captured by the exiting stream channel and associated C-Q relationships. No relationship is found with ASO mean snow depth and fGW ($r^2 = 0.00$, $p = 0.85$). Instead, accounting for area in the calculation of volumetric SWE increases the explanatory power of snow accumulation ($r^2 = 0.68$, $p < 0.05$). Within the ER, topographic slope exerts control on fGW across the basin ($r^2 = 0.46$, $p < 0.03$), and along with relief ($r^2 = 0.59$, $p < 0.01$), appears to be an important predictor of groundwater to streams. Vegetation type and tree density are also significant predictors of fGW. From Figure 5a, the largest volume of SWE spans a mix of barren and low canopy density conifer at elevations 3400 m to 3700 m. Barren locations account for 32% of total SWE within the ER, but the direct relationship of barren area to fGW is weak ($r^2 = 0.18$, $p < 0.2$). In comparison the indirect relationship of fGW with percentage of conifer ($r^2 = 0.81$, $p < 0.001$) and forest canopy density ($r^2 = 0.62$, $p < 0.01$) are stronger.

4.3 Mixing Model Prediction Bias

Table 5 provides Pumphouse mixing model bias calculated from equation 2 for all ten contributing basins for each of the six solutes considered. A negative bias represents an under prediction by the Pumphouse model to replicate observed stream concentrations at a secondary

This article is protected by copyright. All rights reserved.

location, while a positive bias is an over prediction. For stable isotopes, the opposite sign convention holds. Bias for the stable isotopes approaches zero in all basins ($b_j < |0.01|$). Bias in Ca shows little trend among the upper basins: three basins are well predicted with $b_j < |0.01|$ (Quigley, Avery and EBC), four basins are under predicted (EAQ, Rustlers, Bradley, and Marmot) and three basins are over predicted (Rock, Gothic, and Copper). Sr is generally over predicted (b_j = 0.05 to 0.29) by the Pumphouse mixing model but is under predicted (b_j = -0.02 to -0.10) in the Rock, Gothic, and Marmot sub-basins. U is generally over predicted in the upper sub-basins (b_j = 0.02 to 0.40). Only Avery and Copper, draining the eastern reaches of the upper basin, are under predicted with respect to U. SO_4 is nearly ubiquitously under predicted (b_j = -0.04 to -0.57).

5 Discussion

Complex terrain results in spatial and temporal heterogeneity associated with snow accumulation and melt with implications on stream water source as a function of hydrologic partitioning of melt to either runoff or groundwater recharge. Recent evidence suggests high relief watersheds are more dependent on groundwater than initially thought based on older than expected stream flow (Williams et al., 2015; Jasechko et al., 2016), baseflow directly correlated to snow accumulation (Godsey et al., 2014) and hydrograph separation techniques dependent on specific conductance (Miller et al, 2015). We build on these previous studies and others (e.g. Bearup et al., 2014; Cowie et al., 2017) by combining diverse spatial data sets (e.g. NEDS, Landfire, ASO, refer

Author Manuscript

This article is protected by copyright. All rights reserved.

Author Manuscript

to S.1), a robust discharge and precipitation monitoring network, and use of a range in tracers reflecting different mobility and sources. This comprehensive, observational approach helps constrain stream water origination, and highlights those first-order basin properties that enhance recharge to generate more groundwater contributions to streams. In addition, we evaluate where linear mixing assumptions fail to initiate a conceptual model of solute source and transformation as a function of flow path through snow-dominated basins like the ER.

5.1 Factors Controlling Groundwater Contributions

Conceptually, groundwater contributions to a stream are a function of basin characteristics that influence higher rates of infiltration, recharge, and groundwater storage; while those characteristics that promote either high evapotranspiration or runoff reduce contributions. Price (2011) identifies principal geomorphic controls on groundwater flux to streams in terms of geology, surface and subsurface topography, and soil characteristics, but highlights that little consensus occurs on those characteristics that universally promote fGW. Uncertainty in fGW, as defined by observed variability in tracer concentrations, increases seasonally and across sub-basins in the ER as a function of estimated fGW. Despite uncertainty, the relative contributions of end-members remains proportionate across seasons and sub-basins and regression trends with basin characteristics remain largely unaltered. The remaining discussion is therefore limited to the mean annual estimated fGW for each basin.

Within the ER, variation in fGW occurs as functions of basin characteristics associated with snow accumulation, topography and vegetation structure. The importance of snow

This article is protected by copyright. All rights reserved.

Author Manuscript

accumulation on fGW is customarily related to snowmelt as an important source of recharge (Winograd et al., 1988; Godsey et al., 2014). Snow accumulation as defined by average snow depth, however, has no predictive power. Instead volumetric SWE, with its strong dependence on basin area, is the accumulation metric capable of explaining fGW. Scale dependence of groundwater has been observed in previous work. For example, Shaman et al. (2004) found self-similarity in groundwater contributions occurring in basins over a drainage area threshold of 8 km^2 in temperate streams of the US. Likewise, Peralta-Tapia et al. (2015) found topographic controls on groundwater contributions to a Boreal stream network for basins less than 10.6 km^2, above which variability diminished. We observe fGW increases sharply from 0.11 to 0.26 for basins less than 5.5 km^2, after which fGW increases but at a much slower rate to converge toward an annual average contribution of 0.29 at Pumphoue.

Beyond the scaling relationship of water availability via SWE for recharge as a function of drainage area, we find structural controls contributing to fGW variability among all sub-basins independent of size. Topographic controls have long been investigated on travel time distributions (e.g. McGuire et al., 2005), but the influences of subsurface permeability and connectivity likely limit it as a single predictive variable (Tetzlaff et al., 2009). Topographic gradients control the rate of water movement downslope and determine how much water is flushed to stream networks or infiltrated into the soil with potential for deeper recharge. Traditional indices of topography (e.g. TWI = ln(A)/tan(B), A = area, B = slope, Beven and Kierby, 1979) have been used to explain increased groundwater contributions as a function of increased area and decreased slope under the

This article is protected by copyright. All rights reserved.

assumption that the hydraulic gradient approximates surface topography. The influence of slope in the ER is directly related to fGW and this is in contrast to the assumption that steep slopes promote faster response flow, less recharge and less groundwater discharge to streams. Our results fit a regional trend analysis of the UCRB (Rumsey et al., 2015) that found a positive correlation between slope and increased baseflow. For this regional study, the correlation was described as a function of steeper slopes occurring at higher elevations where more precipitation falls. Our study site is limited to high elevation and yet slope still expresses itself as a first-order control on groundwater contributions. A recent global study suggests deeper infiltration in high relief watersheds is perhaps related to increased rock stress and greater propensity for fracturing in the bedrock of these landscapes (Jasechko et al., 2016). Avery has a mean slope approaching 28%, and its anomalous response (Figure 8b) hints that an upper limit of the relationship, likely a function of rock type, may exist, in which gravitational influences on hydraulic gradients overwhelm the potential of deeper percolation.

In addition to these topographic controls, vegetation structure is an important predictor of fGW. LaMalfa and Ryle's (2008) comparative study between aspen and conifer stands demonstrated higher SWE and soil water accumulation in aspen forests. In contrast, ASO-derived snow depths in the ER associated with aspen forests are lower compared to all other vegetation types (Figure S8d), even when accounting for elevation (Figure 5b), as well as slope and aspect (Figure S9). The spatial distribution of aspen at lower elevations and reduced tendency to acquire deep snowpack suggests a lower recharge potential in aspen groves of the ER. Instead, recharge

Author Manuscript

This article is protected by copyright. All rights reserved.

Author Manuscript

potential is greater in the low-density conifer of the upper sub-alpine where the bulk of snow accumulation occurs. The feedbacks between vegetation structure with water and energy budget considerations are well documented. Previous studies have shown snow accumulation is largest in open versus under-canopy conditions because of decreased canopy interception; but open areas are susceptible to scour by winds (Elder et al., 1991) as well as to faster ablation through changes in albedo, increased net shortwave solar radiation, and decreased longwave solar radiation (Musselman et al., 2008; Molotch et al., 2009; Welch et al., 2016). These competing processes of interception and sheltering suggest forests with intermediate tree density, such as the upper sub-alpine in the ER, can retain more snow for longer periods of time and promote greater accumulation (Musselman et al., 2008; Broxton et al., 2015). In addition, the upper sub-alpine forests delay snowmelt initiation, and this is potentially important to generating recharge. Trujillo and Molotch (2014) found sites with larger snow accumulation and later peak SWE tend to experience more rapid snowmelt. The rapid influx of water induces field capacity in the soils and subsequent deep percolation below the root zone to increase relative subsurface flow (Barnhart et al., 2016). Within the ER, melt rates at the higher elevation Schofield site (24.2 mm d^{-1}) occur a month later in 2016 and are nearly double at the rate at the lower elevation Butte site (13.4 mm d^{-1}). Therefore, the propensity to accumulate and hold onto snow later into the year with higher melt rates, points toward upper sub-alpine as the eco-region dominating recharge within the ER and dictating groundwater contributions to streams. Our results are consistent with Zhang et al. (2018) who found approximately half of streamflow in Boulder Creek, CO generated by snowmelt in

This article is protected by copyright. All rights reserved.

the sub-alpine near treeline, with stream water contributions containing a lower proportionate young water fraction relative to the alpine region.

5.2 Critical Zone Influences on Tracer Variability

Simulation bias (Table 5) deviating from zero indicates an inability of the mixing ratios determined at Pumphouse to predict observed stream concentrations along upstream locations in the ER. Inherent assumptions of the EMMA approach, specfically linear mixing and conservative behavior, do not always occur. Instead, stream concentrations are the result of variable sourcing and reactions along specific flow paths that generate non-zero bias. We discuss four potential explanations for why EMMA fails to scale from the Pumphouse site across its upper basin components, and how these processes are related to calculated groundwater flux to streams. Specifically, we address error in EMMA-based partitioning as a function of soil flushing, geology, and carbonate weathering,and biogeochemical transformations in floodplain sediments that modify hillslope contributions of solutes..

5.2.1 Soil and Unsaturated Zone Contributions

As discussed in the section S.4.2, some of the hysteresis in bi-mixing plots, and associated residual error in fitting a linear model (S.3.2), is attributable to the flushing of solutes from the soil and unsaturated zone. To illustrate this point, we aggregated observed ephemeral seep and 10-m hillslope well data and plotted in the PCA defined U-space (Figure 7). November chemistry for unsaturated conditions (H_u) along the hillslope falls far to the left of the deep groundwater

Author Manuscript

This article is protected by copyright. All rights reserved.

signature. This is the consequence of significantly elevated U and SO_4 concentrations in pore waters. In contrast, saturated waters in these hillslope wells (H_s) have lower concentrations than H_u for all solutes considered and converge toward the deep groundwater signature used in EMMA hydrograph separation. The convergence toward a common saturated signature provides some reassurance that use of a single deep groundwater well to define saturated groundwater contributions for all ER basins is a valid strategy. The accumulation of solutes in the unsaturated pore waters, and subsequent flushing during snowmelt is demonstrated by the ephemeral seep data collected in the spring. Seep data collected in May (S_1) prior to peak discharge, and at a break in slope between the hillslope toe and lower floodplain, plots as a mixture of H_s, snow and stream water. Seep data collected later in the runoff period (June) and at a higher elevation on the hillslope (S_2) appears to be a mixture of H_u and H_s chemistry. The mixing reflects snowmelt flushing of solute enrichment within the soil and unsaturated zone and combining with a rapidly rising water table. Including a fourth end-member in EMMA as defined by ephemeral seeps could improve residual analysis (see section S.3.2) while providing insight into the role of seasonal, shallow groundwater contributions and solutes from the hillslope that the current mixing model does not address.

5.2.2 Geologic Considerations

Variability in mixing ratios as expressed in simulated bias is partly attributable to geology. As an example, Gothic is a small basin draining a portion of the western side of the ER. Flow originates within an igneous cirque composed of quartz monzonite from which it then traverses

Author Manuscript

This article is protected by copyright. All rights reserved.

Mancos shale. Gothic stream flow experiences a more rapid rise and attenuation in its hydrograph in response to snowmelt than the other tributaries and fGW to Gothic Creek the lowest in the ER (0.08 to 0.20). Low fGW and associated export of solutes implies limited exposure to mineral grains or insufficient time to reach water-rock equilibrium (Maher, 2011). Rock and Quigley, the other tributaries draining the western edge of the ER domain, have near identical lithologies as Gothic and likewise have low fGW. Despite lower reliance on deep groundwater in these western tributaries, SO_4 is under predicted by the Pumphouse mixing model. In other words, these basins export more SO_4 than the Pumphouse mixing model can predict. We hypothesize that the under prediction is, in part, related to the influence of Mancos shale on SO_4 contributions to stream flow. The shale is composed of quartz, feldspar, interbedded clays, carbonates, sulfates, organic matter, and pyrite (Gaskill et al., 1991). Those basins with greater Mancos mapped at the surface, such as these western tributaries, can explain some of the negative prediction bias but significance is low ($r^2 = 0.19$, $p < 0.25$). Explanatory ability in model bias of SO_4 is improved when the surface quaternary material is not included ($r^2 = 0.52$, $p < 0.01$).

Source rock contributions can also explain prediction bias of U across the upper basin. Felsic magmas tend toward more U than other igneous rocks (Larsen and Gottfried, 1960), and these occur in the ER with quartz monzonite and granodiorite forming several of the highest peaks in the study site. Likewise, the Mancos shale is known to contain U. However, the Morrison Formation (Jm, Figure 2) is host to extensive U mineralization deposited in the Salt Wash, the complex fluvial member of the Morrison Formation (Phoenix, 1958; Tyler and Ethridge, 1983) and

Author Manuscript

This article is protected by copyright. All rights reserved.

the likely dominant source of U in ER tributary waters. The flux of U exiting most tributaries is fairly low (Figure S12-,S13, S20-S23), but baseflow fluxes of U are higher from the eastern basins (Figure S14) and believed attributable to the steeply dipping stratigraphic column shown in Figure 2 that exposes the Morrison Formation in these tributaries. In particular, Copper Creek baseflow concentrations reach 1.2 ppb and account for 38% of the baseflow U mass flux to Pumphouse and this is expressed as a large negative bias. In contrast, positive U bias in most of the other tributaries indicates either a lack of Morrison or insufficient contact with the Morrison Formation. In short, EMMA simulated bias in predicted solutes allows speculation on groundwater contact with specific geologic formations to initiate a conceptual model of groundwater flow paths.

5.2.3 Carbonate Weathering

Winnick et al. (2017) suggested that differential C-Q behavior in solutes at Pumphouse can be explained by carbonate weathering of the Mancos shale. Spring snowmelt results in shallow flow paths, the dominance of carbonic acid weathering, and increased export of DIC. Under baseflow conditions and a deeper water table, infiltrating waters reach calcite saturation prior to passing through an inferred pyrite oxidation front after which sulfuric acid promotes SO_4 export. Using this conceptual model and stoichiometric balance (Li et al., 2008), we can determine the predominance of shallow or deeper flow paths as a function of SO_4 and DIC. Stoichiometrically, end-members for carbonic acid weathering related to shallow flow paths become $HCO_3/(Ca+Mg) = 2$ and $SO_4/(Ca+Mg) = 0$, while end-members for sulfuric acid weathering pertinent to deeper flow paths are $HCO_3/(Ca+Mg) = 1$ and $SO_4/(Ca+Mg) = 0.5$. If we

Author Manuscript

This article is protected by copyright. All rights reserved.

ignore CO_2 outgassing, then SO_4/DIC = 0.5 for sulfuric acid weathering and 0.0 for carbonic acid weathering. Temporal plots of SO_4/DIC are provided in Figure 9 that compare Pumphouse ratios to those tributaries estimated with the lowest (Gothic) and highest (Copper) predicted fGW. All three stream locations experience a shift toward more relative SO_4 during baseflow, but Gothic hovers closer to the carbonic acid end-member year-round to imply shallower flow paths than experienced in the contrasting basins. Copper resides closest to the sulfuric acid weathering end-member to infer, all else equal, longer and deeper flow paths. We acknowledge that the concept of a pyrite oxidation reaction front represents a very specific and singular example that excludes the possibility of other contributions of SO_4 from within the domain, such as the oxidation of pyrite associated with localized sulfide-rich ore deposits or the potential leaching of gypsum-bearing evaporates from the Gothic Formation (refer to Figure 2). Nonetheless, when amassing multiple lines of evidence with respect to tributary hydrographs, solute mass flux, and basin-explicit EMMA calculations of fGW, we see flow path distinctions emerge between the nested domains of Gothic and Copper that bracket the downstream Pumphouse site.

5.2.4 Biogeochemical Transformations

Are biogeochemical transformations across floodplain meanders sufficient to modify hillslope contributions and alter mixing ratios in the analysis? The lower floodplain, as identified in Figure 1, is a low gradient, meandering river system bounded by the EBC and Pumphouse stations with no significant perennial surface inflow other than the ER. The Pumphouse mixing ratios over predict Sr at EBC (0.07) but under predicted SO_4 (-0.11). Both Sr and SO_4 have origins

Author Manuscript

This article is protected by copyright. All rights reserved.

from hillslope weathering yet have different prediction bias. This suggests competing processes between the hillslope and floodplain. A positive Sr prediction error infers Sr is derived at a greater rate from hillslope weathering in the vicinity of the lower floodplain compared to that derived from weathering in the upper basin. Were this the case, we would expect a similar trend in error with SO_4. This is not observed. We put forth the hypothesis that microbial sulfate reduction in the region of the lower floodplain occurs at a higher rate than in the upper basin tributaries. The upper basin tributaries are steep in gradient and we argue more dependent on hillslope processes that provide less opportunity for sulfate reduction. Sulfate reduction requires 1) sufficient organic material for microbial respiration, 2) the presence of sulfate as a terminal electron acceptor, and 3) favorable redox (Hunter et al., 1998) and hydrologic conditions to promote adequate contact time between water and biofilms on the surfaces of sediments (Boano et al., 2010). Hillslopes generally contain well-drained soils and lower organic matter and the organic matter that is present, such as kerogen found in shales, has a lower potential to degrade based on thermodynamic inhibition and thereby a lower potential to be respired by sulfate-reducing bacteria (LaRowe and Van Cappellen, 2011). Additionally, Alewell and Novak (2001) found hillslope dissimilatory sulfate reduction occurs only intermittently and is not an important mechanism of sulfur cycling in a forested watershed despite laboratory conditions indicating a high potential. In contrast, the lower floodplain meanders may offer greater coincidence of all conditions necessary for sulfate reduction. The lower floodplain is a groundwater discharge zone that stabilizes floodplain water tables and provides influxes of SO_4 from carbonate weathering along the hillslope. Meander sinuosity and planimetry

Author Manuscript

This article is protected by copyright. All rights reserved.

Author Manuscript

then regulate the occurrence or absence of the different metabolic pathways such that slow pore velocities or long inter-meander apex distances ensure depletion of oxygen and nitrate to eventually allow sulfate reduction (Boano et al., 2010). Individual basins within the ER exhibit declining baseflow SO_4 concentrations with increased stream length per unit area (r^2= 0.66, p = 0.005; excluding Marmot) to point toward hyporehic losses of SO_4 as a viable mechanism in these mountainous watersheds. While EMMA points toward a relevant statistical signal of sulfate reduction within floodplain sediments with implications on C-Q behavior, a preliminary study of soil samples from the river meanders could not confirm the presence of sulfur-reducing bacteria (Kenwell et al., 2016). At present, more robust and process-oriented experimentation and numerical modeling efforts by the WFSFA are underway to more explicitly address biogeochemical processes along hillslopes and within the floodplain sediments as a function of hydrology.

6. Conclusions

Quantifying stream source as a function of CZ characteristics of topography, geology and vegetation allows better understanding of which watershed sub-components are more dependent on groundwater and potentially buffered from future changes. In addition, hydrologic partitioning of precipitation into rain and snow-derived runoff and groundwater recharge establishes much of the context of solute flux from these basins. Historically, groundwater contributions to stream flow in these mountainous systems were considered minimal based on low storage potential and

This article is protected by copyright. All rights reserved.

steep hydraulic gradients. Our work adds to a growing body of literature to suggest groundwater contributions from these headwater basins may be significant. We find that annually nearly one-third of the exiting stream flow from the ER is attributable to groundwater as reflected by observed C-Q and calculated using the multivariate statistical approach of EMMA. Variability in groundwater contribution to streams across 11 nested-basins are described by SWE, topographic controls of slope and relief as well as vegetation structure. The direct relationship of SWE to groundwater contribution is not a function of snow depth. Rather, SWE's influence on groundwater is scale dependent with variability in fGW more pronounced in sub-basins less than 5.5 km^2 and converging toward a mean annual fGW of 0.29 at larger areas. We find steeper basins and those dominated by upper sub-alpine conditions support more groundwater flux to streams. The upper sub-alpine contains low density, conifer forests that promote snow accumulation, retain snow for longer periods of time and experience faster melt rates once ablation begins. It is argued that all conditions allow a rapid flux of water during melt to reach field capacity to generate recharge. In addition to hydrologic partitioning, we speculate that variability in mixing behavior between individual basins is attributable to CZ feedbacks related to different sources and reactions along subsurface flow paths. EMMA scaling-error points toward contact time with specific geologic units as well as carbonate weathering as a function of seasonality and flow path. Loss of SO_4 across a low gradient, meandering section of the ER, suggests the potential for microbial sulfate reduction in floodplain sediments that is sufficient to modify hillslope contributions and alter mixing ratios in the analysis. Soil flushing of

Author Manuscript

This article is protected by copyright. All rights reserved.

Author Manuscript

concentrated solutes and their mixing with a rapidly rising water table are an important process in the ER in response to snowmelt, but is not included as an end-member in the analysis. Adding this fourth end-member would improve residual analysis and provide insight to this transient yet potentially important source of carbon (Figure S15) and metals from headwater streams. Our use of a comprehensive observation network within the ER is an example of integrating physical hydrology with hydrochemistry and hydrometerology to improve our conceptual understanding of how precipitation is routed and streamflow generated. We find groundwater is an important component in these snow-dominated systems and its contribution to streams is directly linked to CZ characteristics of the basin. While C-Q relationships are controlled by groundwater residence times, no conclusions can be made from the EMMA results with respect to travel times based on multiple degrees of freedom when considering the distribution of ages in the catchment (e.g. Benettin et al., 2015). However, EMMA is a first step to elucidate sourcing and groundwater flow paths in the ER to aid hydrologic conceptualization, guide future observation, and inform numerical model development across a range of scales and key system subcomponents – such as hillslopes, floodplains, and deep groundwater.

Acknowledgements: Work was supported by the Lawrence Berkeley National Laboratory's (LBNL) WFSFA through the US Department of Energy Office of Science, Office of Biological and Environmental Research under contract DE-AC02-05CH11231, and the USGS under Grant/Cooperative Agreement No. (*G16AP00196*). We thank Alexis Navarre-Sitchler and Helen

This article is protected by copyright. All rights reserved.

Malenda of the Colorado School of Mines for their assistance with seep sample collection. In addition, we thank Tetsu Tokunaga and Jiamin Wan of LBNL for generously sharing their hillslope groundwater chemistry data.

Supporting Information: Data and analysis are provided in the following sections, (S.1) Spatial characterization of the East River, (S.2) Stream discharge and geochemical data, (S.3) End-member mixing analysis, (S.4) End-member geochemistry, (S.5) Hydrograph Separation. A poster is provided for Carroll et al (2017), Seasonal stream partitioning and critical zone feedbacks within a Colorado River Headwater Basin, B43E-2166, 2017 Fall Meeting, AGU, New Orleans, LA 11-15, Dec.

References Cited

Alewell, C., and Novak, M. (2001). Spotting zones of dissimilatory sulfate reduction in a forested catchment ^{34}S-the^{35}S approach, *Environmental Pollution*, *112*, 369–377.

Allen, C. D., Macalady, A. K., Chenchouni, H., Bachelet, D., McDowell, N., Vennetier, M., Kitzberger, T., Rigling, A., Breshears, D.D., Hogg, E.H., Gonzalex, P., Fensham, R., Zhang, Z., Castro, J., Demidova, N., Lim, J-H., Allard, G., Running, S.W., Semerci, A., and Cobb, N. (2010). A global overview of drought and heat-induced tree mortality reveals emerging climate change risks for forests. *Forest Ecology and Management*, *259*(4), 660–684. doi:10.1016/j.foreco.2009.09.001.

Anderegg, W. R. L., Kane, J. M., and Anderegg, L. D. L. (2012). Consequences of widespread tree mortality triggered by drought and temperature stress. *Nature Climate Change*, *3*(1), 30–36. doi:10.1038/nclimate1635.

Apodaca, L. E. (1997). Analysis of Ground-Water-Quality Data of the Upper Colorado River

Author Manuscript

This article is protected by copyright. All rights reserved.

Author Manuscript

Basin, Water Years 1972-92. *U.S Geological Survey Water-Resources Investigation Report, 97-4240*, 1–37.

Arnold, J. G., Allen, P. M., Muttiah, R., and Bernhardt, G. (1995). Automated baseflow separation and recession analysis techniques. *Ground Water*, *33*(6), 1010–1018.

Barnhart, T. B., Molotch, N. P., Livneh, B., Harpold, A. A., Knowles, J. F., and Schneider, D. (2016). Snowmelt rate dictates streamflow. *Geophysical Research Letters*, *43*(15), 8006–8016. doi:10.1002/2016GL069690.

Bearup, L. A, Maxwell, R. M., Clow, D. W., and Mccray, J. E. (2014). Hydrological effects of forest transpiration loss in bark beetle-impacted watersheds. *Nature Climate Change*, *4*(6), 481–486. doi:10.1038/NCLIMATE2198.

Beck, H. E., Van Dijk, A. I. J. M., Miralles, D. G., De Jeu, R. A. M., Bruijnzeel, L. A., McVicar, T. R., and Schellekens, J. (2013). Global patterns in base flow index and recession based on streamflow observations from 3394 catchments. *Water Resources Research*, *49*(12), 7843–7863. doi:10.1002/2013WR013918.

Beven, K., and Kierby, M. J. (1979). A physically-based, variable contributing area model of basin hydrology. *Hydrological Sciences Bulletin*, *24*(1), 43–69.

Benettin, P., Kirchner, J.W., Rinaldo, A, and Botter, G. (2015). Modeling chloride transport using travel time distributions at Plynlimon, Wales. *Water Resources Research*, 51(5),3259-3276.

Biederman, J. A., Somor, A. J., Harpold, A. A., Gutmann, E. D., Breshears, D. D., Troch, P. A., Gochis, D.J., Scott, R.L., Meddens, A.J.H., and Brooks, P. D. (2015). Recent tree die-off has little effect on streamflow in contrast to expected increases from historical studies. *Water Resources Research*, *51*(12), 9775–9789. doi:10.1002/2015WR017401.

Boano, F., Demaria, A., Revelli, R., and Ridolfi, L. (2010). Biogeochemical zonation due to intrameander hyporheic flow. *Water Resources Research*, *46*(2), 1–13. doi:10.1029/2008WR007583.

Brooks, P. D., Chorover, J., Fan, Y., Godsey, S. E., Maxwell, R. M., McNamara, J. P., and

This article is protected by copyright. All rights reserved.

Author Manuscript

Tague, C. (2015). Hydrologic partitioning in the critical zone: recent advances and opportunities for developing transferable understanding of water cycle dynamics. *Water Resources Research, 51,* 6973–6987. doi:10.1002/2015WR017039.

Brooks, P. D., Chorover, J., Fan, Y., Godsey, S. E., Maxwell, R. M., McNamara, J. P., and Tague, C. (2015). Hydrological partitioning in the critical zone: Recent advances and opportunities for developing transferable understanding of water cycle dynamics. *Water Resources Research, 51,* 6973–6987. doi:10.1002/ 2015WR017039.

Broxton, P. D., Harpold, A. A., Biederman, J. A., Troch, P. A., Molotch, N. P., and Brooks, P. D. (2015). Quantifying the effects of vegetation structure on snow accumulation and ablation in mixed-conifer forests. *Ecohydrology*, *8*(6), 1073–1094. doi:10.1002/eco.1565.

Carroll, R. W. H., Huntington, J. L., Snyder, K. A., Niswonger, R. G., Morton, C., and Stringham, T. K. (2017). Evaluating mountain meadow groundwater response to Pinyon-Juniper and temperature in a great basin watershed. *Ecohydrology, 10*(1), 1–18. doi:10.1002/eco.1792.

Clow, D. W. (2010). Changes in the Timing of Snowmelt and Streamflow in Colorado: A Response to Recent Warming. *Journal of Climate, 23*(9), 2293–2306. doi:0.1175/2009JCLI2951.1.

Dietermann, N., and Weiler, M. (2013). Spatial distribution of stable water isotopes in alpine snow cover. *Hydrology and Earth System Sciences, 17,* 2657–2668. doi:10.5194/hess-17-2657-2013.

Edburg, S. L., Hicke, J. A., Brooks, P. D., Pendall, E. G., Ewers, B. E., Norton, U., Gochis, D.J., Gutmann, E.D., and Meddens, A. J. H. (2012). Cascading impacts of bark beetle-caused tree mortality on coupled biogeophysical and biogeochemical processes. *Frontiers in Ecology and the Environment, 10*(8), 416–424. doi:10.1890/110173.

Elder, K., Dozier, J., and Michaelsen, J. (1991). Snow accumulation and distribution in an alpine watershed. *Water Resources Research, 27,* 1451–1552.

Gaskill, D. L., Mutschler, F. E., Kramer, J. H., Thomas, J. A., and Zahony, S. G. (1991).

This article is protected by copyright. All rights reserved.

Author Manuscript

Geologic map of the Gothic Quadrangle, Gunnison County, Colorado.

Godsey, S. E., Kirchner, J. W., and Clow, D. W. (2009). Concentration-discharge relationships reflect chemostatic characteristics of US catchments. *Hydrological Processes*, *23*, 1844–1864. doi:10.1002/hyp.7317.

Godsey, S. E., Kirchner, J. W., and Tague, C. L. (2014). Effects of changes in winter snowpacks on summer low flows: Case studies in the Sierra Nevada, California, USA. *Hydrological Processes*, *28*(19), 5048–5064. doi:10.1002/hyp.9943.

Hoerling, M. P., Dettinger, M., Wolter, K., Lukas, J., Eischeid, J., Rama, N., … Kunkel, K. E. (2013). Present Weather and Climate: Evolving Conditions. In G. Garfin, A. Jardine, R. Merideth, M. Black, and S. LeRoy (Eds.), *A report by the Southwest Climate Alliance* (pp. 74–100). Washington, DC: Island Press..

Hooper, R. P. (2003). Diagnostic tools for mixing models of stream water chemistry. *Water Resources Research*, *39*(3), 1055. doi:10.1029/2002wr001528.

Hunter, K. S., Wang, Y., and Van Cappellen, P. (1998). Kinetic modeling of microbially-driven redox chemistry of radionuclides in subsurface environments: Coupling transport, microbial metabolism and geochemistry. *Journal of Hydrology*, *209*, 53–80.

IPCC. (2014). Technical summary. *Climate Change 2014: Impacts, Adaptation and Vulnerability. Part A: Global and Sectorial Aspects. Contribution of Working Group II to the 5th Assessment Report of the Intergovernmental Panel on Climate Change*, 60.

Jasechko, S., Kirchner, J. W., Welker, J. M., and McDonnell, J. J. (2016). Substantial proportion of global streamflow less than three months old. *Nature Geoscience*, *9*(2), 126–129. doi:10.1038/ngeo2636

Kenwell, A., Navarre-Sitchler, A., Prugue, R., Spear, J. R., Hering, A. S., Maxwell, R. M., Carroll, R.W.H., and Williams, K. H. (2016). Using geochemical indicators to distinguish high biogeochemical activity in floodplain soils and sediments. *Science of the Total Environment*, *563-564*, 386–395. doi:10.1016/j.scitotenv.2016.04.014.

Kirchner, J. W. (2003). A double paradox in catchment hydrology and geochemistry.

This article is protected by copyright. All rights reserved.

Hydrological Processes, *17*(4), 871–874. doi:10.1002/hyp.5108

Kirchner, J. W. (2006). Getting the right answers for the right reasons: linking measurements, analyses, and models to advance the science of hydrology. *Water Resources Research*, *42*. doi:10.1029/2005WR004362.

Kirchner, J. W. (2009). Catchments as simple dynamical systems: catchment characterization, rainfall-runoff modeling, and doing hydrology backward. *Water Resources Research*, *45*. doi:10.1029/2008WR006912.

Kormos, P. R. (2005). *Accounting for time and space variations of δ18O in a snowmelt isotopic hydrograph separation in the Boise Front*. Boise State University, Boise Idaho.

Kormos, P. R., Marks, D., McNamara, J. P., Marshall, H. P., Winstral, A., and Flores, A. N. (2014). Snow distribution, melt and surface water inputs to the soil in the mountain rain–snow transition zone. *Journal of Hydrology*, *519*, 190–204. doi:10.1016/j.jhydrol.2014.06.051.

Krause, S., Lewandowski, J., Grimm, N. B., Hannah, D. M., Pinay, G., McDonald, K., Marti, E., Argerich, A., Pfister, L., Klaus, J., Battin, T., Larned, S.T., Schelker, J., Fleckenstein, J., Schmidt, C., Rivett, M.O., Watts, G., Sabater, F., Sorolla, A., and Turk, V. (2017). Ecohydrological interfaces as hotspots of ecosystem processes. *Water Resources Research*, doi:10.1002/2016WR019516.

LaMalfa, E. M., and Ryle, R. (2008). Differential snowpack accumulation and water dynamics in aspen and conifer communities: Implications for water yield and ecosystem function. *Ecosystems*, *11*(4), 569–581. doi:10.1007/s10021-008-9143-2.

Landfire. 2008, Existing Vegetation Type Layer, LANDFIRE 1.1.0, U.S. Department of the Interior, Geological Survey. Accessed 20 October 2017 at http://landfire.cr.usgs.gov/viewer/.

LaRowe, D. E., and Van Cappellen, P. (2011). Degradation of natural organic matter: A thermodynamic analysis. *Geochimica et Cosmochimica Acta*, *75*(8), 2030–2042.

Author Manuscript

This article is protected by copyright. All rights reserved.

Author Manuscript

doi:10.1016/j.gca.2011.01.020.

Larsen, E. S. 3rd, and Gottfried, D. (1960). Uranium and Thorium in selected suites of igneous rocks. *American Journal of Science*, *258*(A), 151–169. Retrieved from http://earth.geology.yale.edu/~ajs/1960/ajs_258A_11.pdf/151.pdf.

Li, D., Wrzesien, M. L., Durand, M., Adam, J., and Lettenmaier, D. P. (2017). How much runoff originates as snow in the western United States, and how will that change in the future? *Geophysical Research Letters*, 6163–6172. doi:10.1002/2017GL073551.

Li, S.-L., Calmels, D., Han, G., Gaillardet, J., and Liu, C.-Q. (2008). Sulfuric acid as an agent of carbonic weathering constrained by $\delta^{13}C$ DIC: examples from Southwest China. *Earth and Planetary Science Letters*, *270*, 189–199.

Lukas, J., Barsugli, J., Doeksen, N., Rangwala, I., and Wolter, K. (2014). Climate Change in Colorado. *University of Colorado Boulder*, 1–108.

Maher, K. (2011). The role of fluid residence time and topographic scales in determining chemical fluxes from landscapes. *Earth and Planetary Science Letters*, *312*(1-2), 48–58. doi:10.1016/j.epsl.2011.09.040.

Markstrom, S. L., Hay, L. E., Ward-Garrison, C. D., Risley, J. C., Battaglin, W. a, Bjerklie, D. M., Chase, K.J., Christiansen, D.E., Dudley, R.W., Hunt, R.J., Koczot, K.M., Mastin, M.C., Regan, R.S., Viger, R.J., VIning, K.C., and Walker, J. F. (2012). Integrated watershed-scale response to climate change for selected basins across the United States. U.S. Geological Survey Scientific Investigations Report 2011–5077, 143.

Mast, M. A., Kendall, C., Campbell, D. H., Clow, D. W., and Black, J. (1995). Determination of hydrologic pathways in an alpine-subalpine basin using isotopic and chemical tracers, Loch Vale Watershed, Colorado, USA. *Biogeochem. Seas. Snow-Covered Catchments Proceedings Boulder Symp. IAHS Pulication, 228*.

McCabe, G. J., Wolock, D. M., Pederson, G. T., Woodhouse, C. A., and McAfee, S. (2017). Evidence that Recent Warming is Reducing Upper Colorado River Flows. *Earth Interactions*, EI–D–17–0007.1. doi:10.1175/EI-D-17-0007.1

This article is protected by copyright. All rights reserved.

Author Manuscript

McGuire, K. J., McDonnell, J. J., Weiler, M., Kendall, C., McGlynn, B. L., Welker, J. M., and Seibert, J. (2005). The role of topography on catchment-scale water residence time. *Water Resources Research*, *41*(5). doi:10.1029/2004WR003657.

Melcher, N.B., and Walker, J.F. (1992). Evaluation of selected methods for determining streamflow during periods of ice effect. U.S. Geological Survey Water Supply-Paper 2378. 53 pp.

Miller, M. P., Buto, S. G., Susong, D. D., and Rumsey, C. A. (2016). The importance of base flow in sustaining surface water flow in the Upper Colorado River Basin. *Water Resources Research*, *52*(5), 3547–3562. doi:10.1002/2015WR017963.

Miller, M. P., Johnson, H. M., Susong, D. D., and Wolock, D. M. (2015). A new approach for continuous estimation of baseflow using discrete water quality data: Method description and comparison with baseflow estimates from two existing approaches. *Journal of Hydrology*, *522*, 203–210. doi:10.1016/j.jhydrol.2014.12.039.

Molotch, N. P., Brooks, P. D., Burns, S. P., Litvak, M., Monson, R. K., McConnell, J. R., and Musselman, K. (2009). Ecohydrological controls on snowmelt partitioning in mixed-conifer sub-alpine forests. *Ecohydrology*, *2*, 129–142. http://doi.org/DOI: 10.1002/eco.48.

MRI - Mountain Research Initiative. (2015). Elevation-dependent warming in mountain regions of the world. *Nature Clim. Change*, *5*(5), 424–430. doi:10.1038/nclimate2563\r.

Musselman, K. N., Molotch, N. P., and Brooks, P. D. (2008). Effects of vegetation on snow accumulation and ablation in a mid-latitude sub-alpine forest. *Hydrological Processes*, *22*(15), 2767–2776. doi:10.1002/hyp.7050.

Nathan, R. J., and McMahon, T. A. (1990). Evaluation of automated techniques for baseflow and recession analysis. *Water Resources Research*, *26*(7), 1465–1473.

Painter, T. H., Berisford, D. F., Boardman, J. W., Bormann, K. J., Deems, J. S., Gehrke, F., Hedrick, A., Joyce, M., Laidlaw, R., Marks, D., Mattmann, C., McGurk, B., Ramirez, P., Richardson, M., Skiles, S.M., Seidel, F.C., and Winstral, A. (2016). The Airborne Snow Observatory: Fusion of scanning lidar, imaging spectrometer, and physically-based

This article is protected by copyright. All rights reserved.

Author Manuscript

modeling for mapping snow water equivalent and snow albedo. *Remote Sensing of Environ.ment*, *184*, 139–152. doi:10.1016/j.rse.2016.06.018.

Peralta-Tapia, A., Sponseller, R. A., Agren, A., Tetzlaff, D., Soulsby, C., and Laudon, H. (2015). Scale-dependent groundwater contributions influence patterns of winter baseflow stream chemistry in boreal catchments. *Journal of Geophysical Research: Biogeosciences*, *120*(361), 1–13. doi:10.1002/2014JG002872.

Perdrial, J. N., McIntosh, J., Harpold, A., Brooks, P. D., Zapata-Rios, X., Ray, J., Meixner, T., Kanduc, T., Litvak, M., Troch, P.A., and Chorover, J. (2014). Stream water carbon controls in seasonally snow-covered mountain catchments: impact of inter-annual variability of water fluxes, catchment aspect and seasonal processes. *Biogeochemistry*, *118*(1-3), 273–290. doi:10.1007/s10533-013-9929-y.

Phoenix, D. A. (1958). Uranium deposits under conglomerate sandstone of the Morrison Formation, Colorado and Utah. *GSA Bulletin*, *69*(4), 403–418. doi:10.1130/0016-7606(1958)69[403:UDUCSO]2.0.CO;2

Price, K. (2011). Effects of watershed topography, soils, land use, and climate on baseflow hydrology in humid regions: a review. *Progress in Physical Geography*, *35*(465-492). doi:10.1177/0309133311402714

Rumsey, C. A., Miller, M. P., Susong, D. D., Tillman, F. D., and Anning, D. W. (2015). Regional Studies Regional scale estimates of baseflow and factors influencing baseflow in the Upper Colorado River Basin. *Journal of Hydrology*, *4*, 91–107.

Santhi, C., Allen, P. M., Muttiah, R. S., Arnold, J. G., and Tuppad, P. (2008). Regional estimation of base flow for the conterminous United States by hydrologic landscape regions. *Journal of Hydrology*, *351*(1-2), 139–153. doi:10.1016/j.jhydrol.2007.12.018

Shaman, J., Stieglitz, M., and Burns, D. (2004). Are big basins just the sum of small catchments? *Hydrological Processes*, *18*(16), 3195–3206. doi:10.1002/hyp.5739

Taylor, R. G., Scanlon, B., Döll, P., Rodell, M., van Beek, R., Wada, Y., Longuevergne, L., Leblanc, M., Famiglietti, J.S., Edmunds, M., Konikow, L., Green, T.R., Chen, J., Taniguchi,

This article is protected by copyright. All rights reserved.

Author Manuscript

M., Bierkens, M.F.P., MacDonald, A., Fan, Y., Maxwell, R.M., Yechieli, Y., Gurdak, J.J., Alle, D.M., Shamsudduha, M., Hiscock, K., Yeh, P.J-F., Holman, I., and Treidel, H. (2012). Ground water and climate change. *Nature Climate Change*, *3*(4), 322–329. doi:10.1038/nclimate1744.

Tetzlaff, D., Seibert, J., McGuire, J., Laudon, H., Burns, D. A., Dunn, S. M., and Soulsby, C. (2009). How does landscape sturcture influence catchment scale transit time across different geomorphic provinces? *Hydrological Processes*, *23*, 945–953.

Trujillo, E., and Molotch, N. P. (2014). Snowpack regimes of the Western United States. *Water Resources Research*, *50*(7), 5611–5623. doi:10.1002/2013WR014753.

Tyler, N., and Ethridge, F. G. (1983). Depositional setting of the Salt Wash Member of the Morrison Formation, Southwest Colorado. *Journal of Sedimentary Petrology*, *53*(1), 67–82.

Vano, J. A., Das, T., and Lettenmaier, D. P. (2012). Hydrologic Sensitivities of Colorado River Runoff to Changes in Precipitation and Temperature. *Journal of Hydrometeorology*, *13*(3), 932–949. doi:10.1175/JHM-D-11-069.1.

Welch, C. M., Stoy, P. C., Rains, F. A., Johnson, A. V., and Mcglynn, B. L. (2016). The impacts of mountain pine beetle disturbance on the energy balance of snow during the melt period. *Hydrological Processes*, *30*(4), 588–602. h doi:10.1002/hyp.10638.

Wilcox, B. P., and Huang, Y. (2010). Woody plant encroachment paradox: Rivers rebound as degraded grasslands convert to woodlands. *Geophysical Research Letters*, *37*(7), 1–5. doi:10.1029/2009GL041929.

Williams, M. W., Hood, E., Molotch, N. P., Caine, N., Cowie, R., and Liu, F. (2015). The 'Teflon basin' myth: hydrology and hydrochemistry of a seasonally snow-covered catchment. *Plant Ecology and Diversity*, *8*(5-6), 639-661.

Winchell, T. S., Barnard, D. M., Monson, R. K., Burns, S. P., and Molotch, N. P. (2016). Earlier snowmelt reduces atmospheric carbon uptake in midlatitude subalpine forests. *Geophysical Research Letters*, *43*(15), 8160–8168. doi:10.1002/2016GL069769.

Winnick, M. J., Carroll, R. W. H., Williams, K. H., Maxwell, R. M., Dong, W., and Maher, K.

This article is protected by copyright. All rights reserved.

(2017). Snowmelt controls on concentration-discharge relationships and the balance of oxidative and acid-base weathering fluxes in an alpine catchment, East River, Colorado. *Water Resources Research*, *53*. doi:10.1002/2016WR019724.

Winograd, I. J., Riggs, A. C., and Coplen, T. B. (1988). The relative contributions of summer and cool-season preciptiation to groundwater recharge, Spring Mountains, Nevada, USA. *Hydrogeology Journal*, *6*(1), 77–93.

Wymore, A. S., Brereton, R. L., Ibarra, D. E., Maher, K., and McDowell, W. H. (2017). Critical zone structure controls concentration-discahrge relationships and solute generation in forested tropical montane watersheds. *Water Resources Research*. doi:10.1002/2016WR020016.

Zhang, Q., Knowles, J.F., Barnes, R.T., Cowie, R.M., Rock, N., Williams, M.W. (2018). Surface and subsurface water contributions to streamflow from a mesoscale watershed in complex mountain terrain. *Hydrological Processes*. doi: 10.1002/hyp.11469.

Author Manuscript

This article is protected by copyright. All rights reserved.

Author Manuscript

Table 1. ER basin characteristics

Basin ID	name	Area[a]	Elev[b]	Relief[b]	Slope[b]	Aspect[b]	SWE[c]	Mancos[d]	Vegetation Type[e]			Tree Density[f]
									Barren	Conifer	Aspen	
1	EAQ[h]	5.27	3349	900	24	127	3.02	0.70	0.25	0.58	0.04	23
2	Quigley	2.55	3380	915	22	85	1.62	0.62	0.23	0.61	0.01	26
3	Rustlers	14.78	3490	1,118	22	196	8.51	0.08	0.24	0.54	0.00	18
4	Bradley	3.82	3504	1,107	22	242	2.08	0.01	0.41	0.50	0.00	20
5	Rock	3.57	3375	931	16	119	2.07	0.68	0.08	0.72	0.00	32
6	Gothic	0.90	3379	875	20	164	0.51	0.34	0.23	0.70	0.00	33
7	Marmot	0.38	3152	544	18	232	0.11	0.00	0.02	0.87	0.06	42
8	Avery	0.60	3390	916	28	243	0.25	0.00	0.34	0.52	0.02	21
9	Copper	23.67	3528	1,242	25	199	13.02	0.01	0.50	0.36	0.02	14
10	EBC[h]	69.81	3421	1,251	22	182	36.92	0.18	0.32	0.49	0.04	20
11[g]	Pumphouse[h]	84.73	3346	1,364	21	175	41.05	0.18	0.27	0.48	0.09	22

[a]units of km^2

[b]mean values for elevation (m), slope (%) and aspect (degrees); relief (m)

[c]described in section 3.3 (Mm^3)

[d]fraction of basin area mapped at surface

[e]fraction of basin area

[f]area weighted %

[g]EMMA reference cite

[h]occur on main stem of the East River (ER)

This article is protected by copyright. All rights reserved.

Author Manuscript

This article is protected by copyright. All rights reserved.

Table 2. Water year 2016 flow characteristics of ER basins. Q = average discharge; Q_b = average baseflow; Q_p = peak discharge.

Basin ID	name	Q	Q_b	Q_p		% Pumphouse	
		$m^3 s^{-1}$		$m^3 s^{-1}$	date	Q	Q_b
1	EAQ	0.12	0.02	1.68	10-Jun	7.5	3.6
2	Quigley	0.04	0.02	0.39	10-Jun	2.3	3.9
3	Rustlers	0.35	0.07	4.19	8-Jun	21.5	15.4
4	Bradley	0.06	0.01	0.68	11-Jun	3.5	1.9
5	Rock	0.04	0.01	0.51	5-Jun	2.5	2.5
6	Gothic	0.01	0.0003	0.26	11-Jun	0.6	0.1
7	Marmot	0.01	0.00	0.07	7-Jun	0.5	0.6
8	Avery	0.02	0.01	0.06	21-May	1.2	3.1
9	Copper	0.41	0.11	3.47	10-Jun	25.4	25.0
10	EBC*	1.06	0.26	10.90	10-Jun	65.1	56.0
11	Pumphouse	1.63	0.46	12.20	11-Jun	1.0	1.0

*EBC flows are given as the sum of all measured upstream contributions (1-9)

Author Manuscript

This article is protected by copyright. All rights reserved.

Table 3. Fraction of Pumphouse stream flow source contributions based on three end-members for baseflow (b), rising limb (r), falling limb (f), and monsoon (m) hydrographic periods. GW = deep groundwater.

Period	fGW	fSnow	fRain
b	0.43	0.48	0.09
r	0.22	0.69	0.08
f	0.18	0.74	0.08
m	0.31	0.53	0.16

Author Manuscript

This article is protected by copyright. All rights reserved.

Table 4. Groundwater fractions of streamflow (fGW) for ER sub-basins. Fractions given as mean with uncertainty provided as (minimum – maximum).

Basin	baseflow (b)	rising (r)	falling (f)	monsoon (m)
EAQ	0.37 (0.29-0.50)	0.23 (0.20-0.29)	0.22 (0.18-0.28)	0.32 (0.26-0.41)
Quigley	0.28 (0.22-0.28)	0.11 (0.09-0.14)	0.16 (0.13-0.20)	0.25 (0.20-0.32)
Rustlers	0.33 (0.26-0.45)	0.21 (0.17-0.26)	0.16 (0.13-0.20)	0.26 (0.21-0.34)
Bradley	0.31 (0.25-0.42)	0.21 (0.17-0.26)	0.17 (0.14-0.21)	0.24 (0.19-0.31)
Rock	0.20 (0.16-0.27)	0.09 (0.17-0.11)	0.09 (0.07-0.11)	0.18 (0.14-0.23)
Gothic	0.17 (0.13-0.23)	0.07 (0.06-0.09)	0.07 (0.06-0.09)	0.15 (0.12-0.20)
Marmot	0.34 (0.27-0.46)	0.20 (0.17-0.25)	0.17 (0.14-0.21)	0.28 (0.22-0.36)
Avery	0.21 (0.17-0.29)	0.15 (0.12-0.18)	0.14 (0.12-0.18)	0.18 (0.15-0.23)
Copper	0.50 (0.39-0.68)	0.27 (0.22-0.34)	0.17 (0.14-0.22)	0.32 (0.26-0.41)
EBC	0.41 (0.32-0.55)	0.23 (0.19-0.28)	0.16 (0.14-0.20)	0.29 (0.24-0.38)
Pumphouse	0.43 (0.34-0.58)	0.22 (0.19-0.28)	0.18 (0.15-0.23)	0.31 (0.25-0.40)

Author Manuscript

This article is protected by copyright. All rights reserved.

Table 5. ER upper basin bias calculated using the Pumphouse mixing space.

ID	Basin	Ca	Sr	U	SO_4	δ^2H	$\delta^{18}O$
1	EAQ	-0.21	0.05	0.29	-0.07	0.002	-0.002
2	Quigley	0.01	0.05	0.40	-0.57	0.004	-0.005
3	Rustlers	-0.08	0.15	0.11	-0.23	0.005	-0.001
4	Bradley	-0.18	0.29	0.22	-0.40	0.009	-0.001
5	Rock	0.11	-0.05	0.25	-0.41	-0.003	-0.001
6	Gothic	0.15	-0.09	0.02	-0.13	-0.005	0.001
7	Marmot	-0.27	-0.02	0.40	0.04	0.001	-0.002
8	Avery	0.00	0.18	-0.22	-0.04	0.002	0.004
9	Copper	0.17	0.10	-0.27	-0.13	0.004	0.000
10	EBC	0.01	0.07	-0.01	-0.11	0.001	0.001

Author Manuscript

This article is protected by copyright. All rights reserved.

Author Manuscript

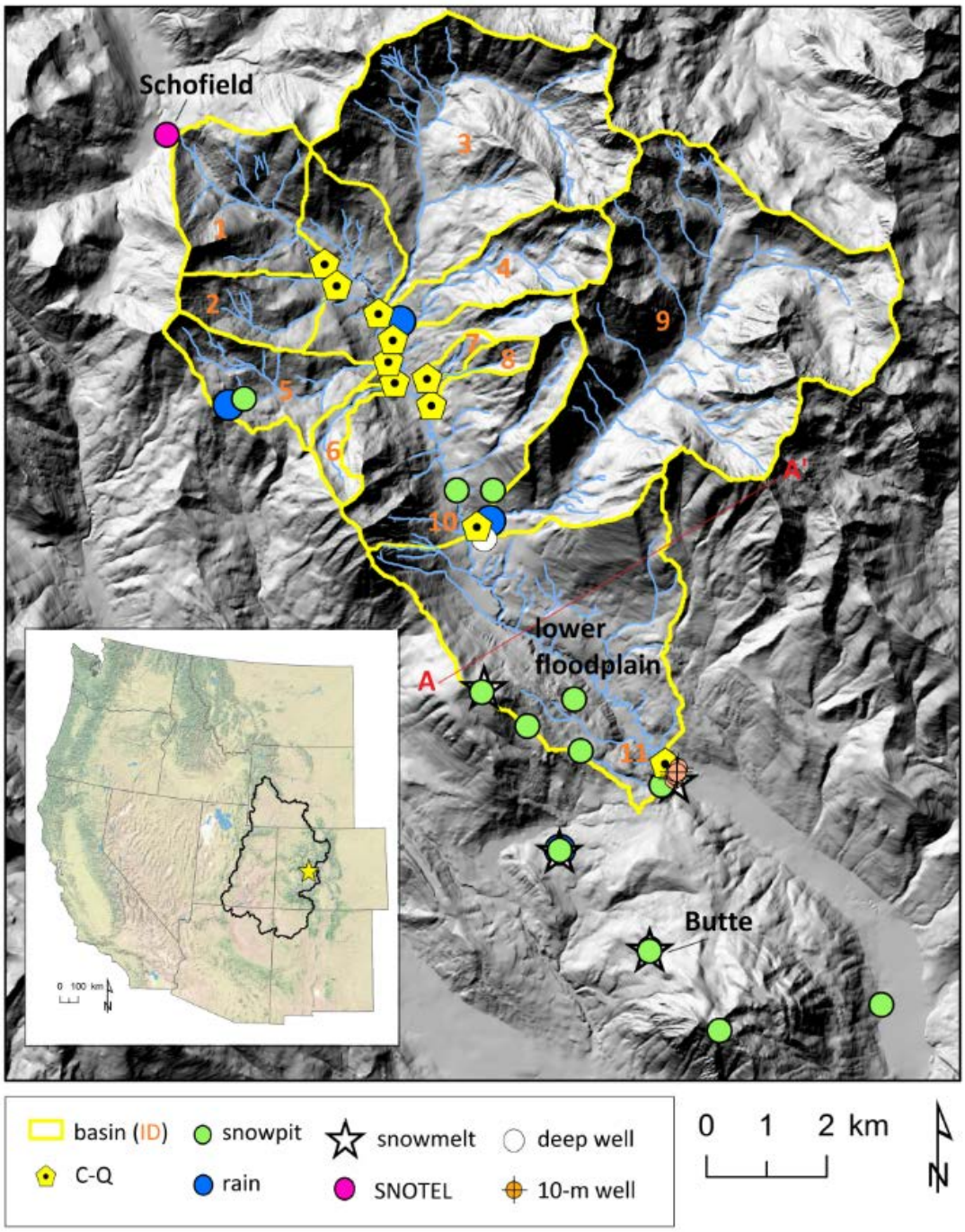


Figure. 1. ER study site delineated with sampling locations provided. Basin identification numbers provided

This article is protected by copyright. All rights reserved.

in Table 1. Stream discharge-concentration sites shown as C-Q, with the Butte and Schofield SNOTEL sites
identified by name. Geologic cross section A-A' provided in Figure. 2. (Inset) Location of the ER indicated
with a star within the UCRB (black outline) in the context of the western US.

Author Manuscript

This article is protected by copyright. All rights reserved.

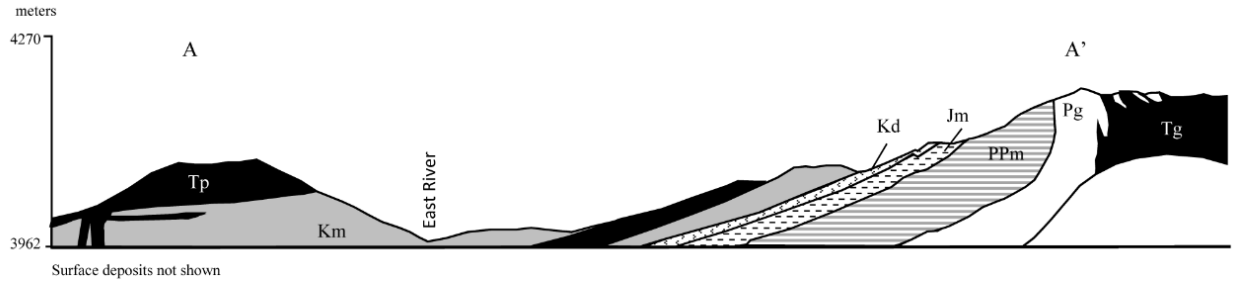


Figure 2. Geologic cross section A-A' traversing the lower floodplain of the ER (Figure 1). Geologic units: Tp
and Tg= Oligocene quartz monzonite and granodiorite, respectively; Km = Cretaceous Mancos Formation;
Kd = Cretaceous Dakota Sandstone; Jm = Jurassic Morrison Formation; PPm = Permian/Pennsylvanian
Maroon Formation; Pg = Pennsylvanian Gothic Formation. Jurassic Entrada Sandstone (Je) not shown but
occurs as thin unit at the interface of Jm and PPm. Figure modified from Gaskill et al. (1991).

Author Manuscript

This article is protected by copyright. All rights reserved.

Author Manuscript

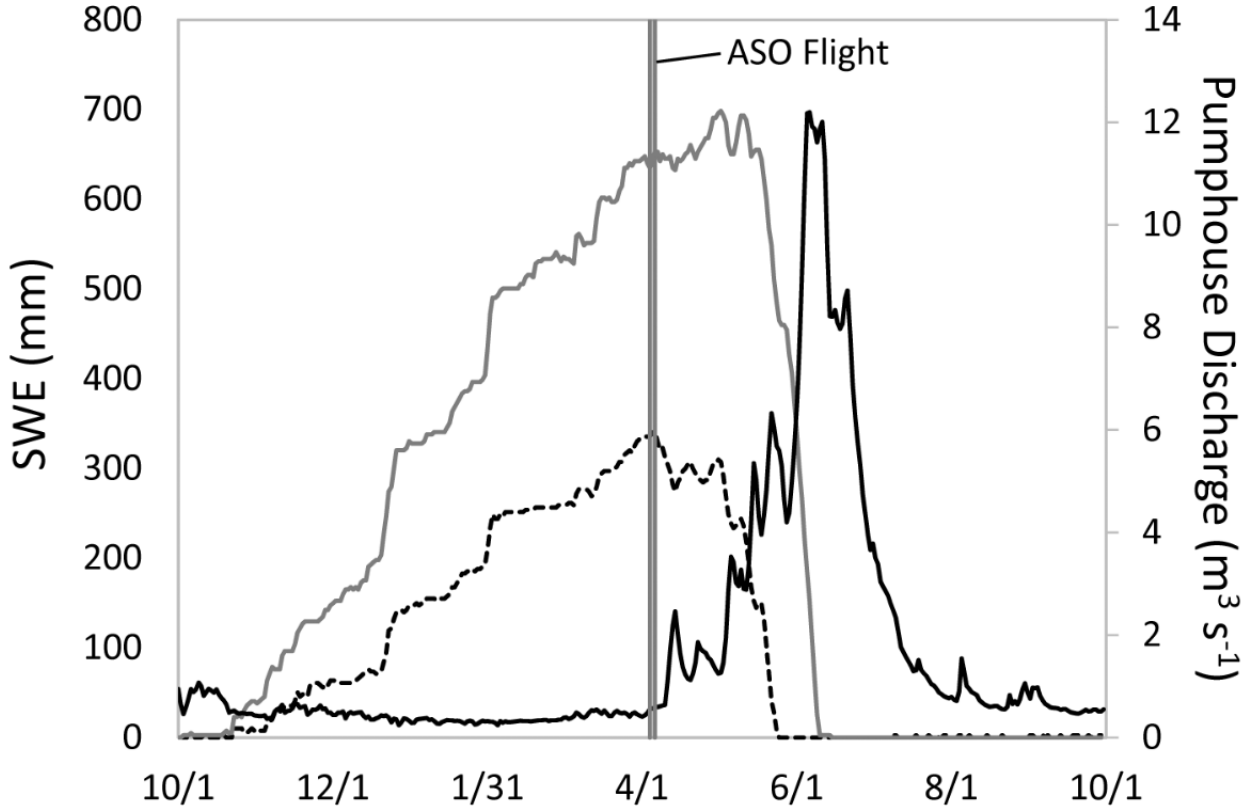
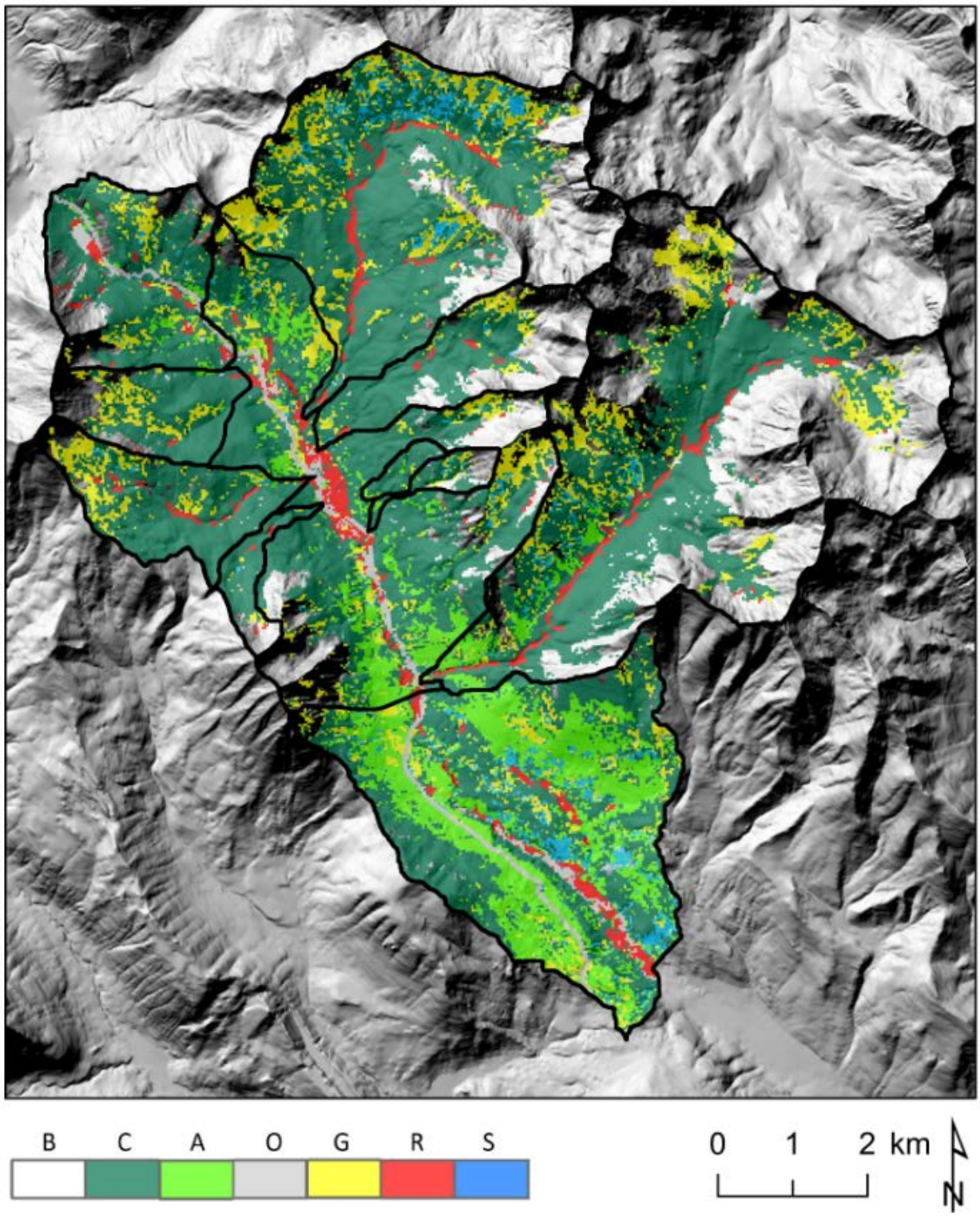


Figure 3. Water year 2016 snow water equivalent (SWE) at the two SNOTEL sites (Schofield as solid gray
and Butte as dashed gray) and daily stream discharge at Pumphouse (solid black). Dates of ASO flight
marked (ASO snow depth data presented in section S.1.3).

This article is protected by copyright. All rights reserved.

Author Manuscript



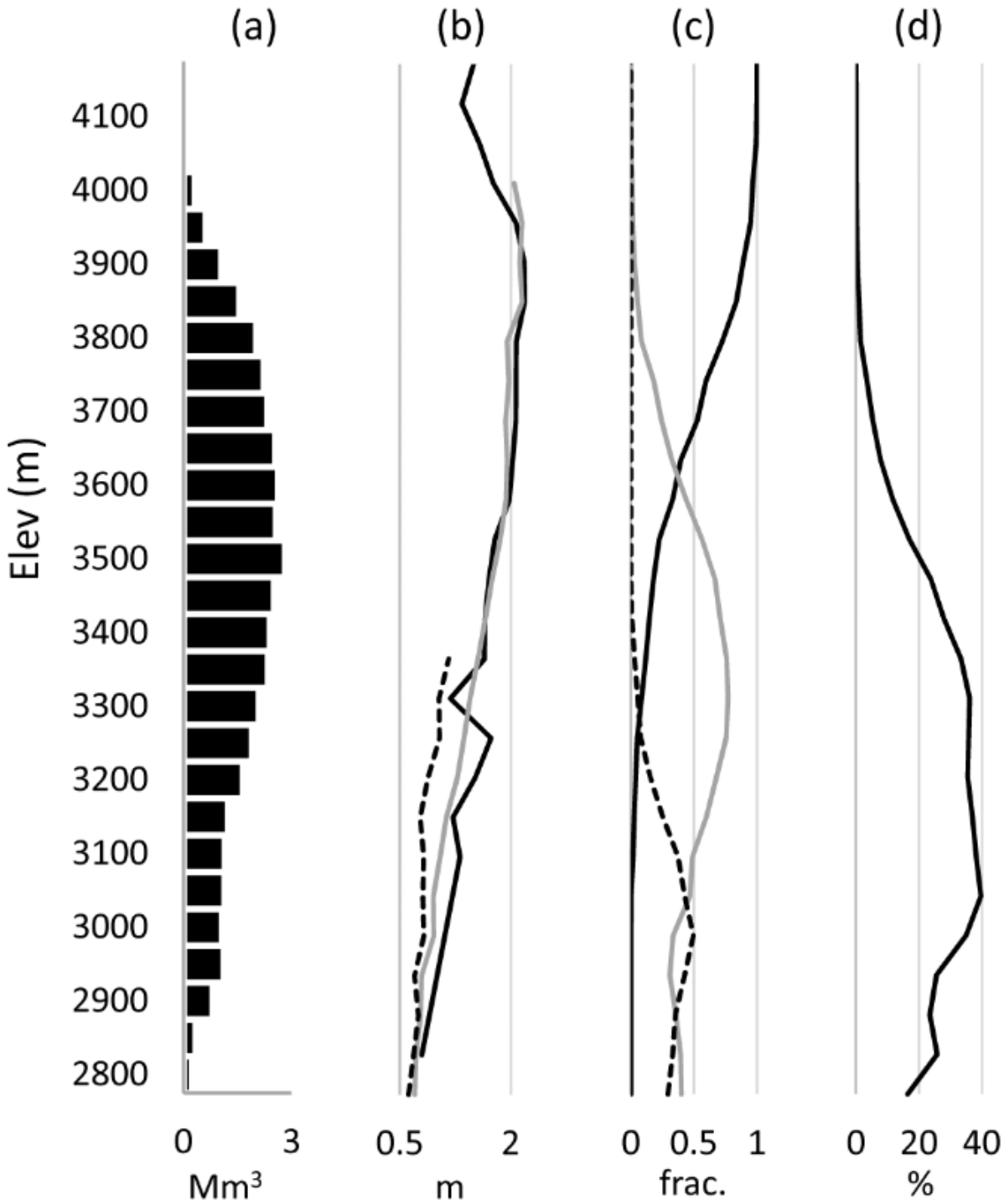
This article is protected by copyright. All rights reserved.

Figure 4. Spatial distribution of vegetation type. B = Barren/Alpine; C = Conifer; A = Aspen; O = Other; G =
Grass; R = Riparian; and S = Shrub.

Author Manuscript

This article is protected by copyright. All rights reserved.

Author Manuscript



This article is protected by copyright. All rights reserved.

Figure 5. ER elevational trends in (a) SWE, Mm3, (b) snow depth by vegetation type, m, (c) vegetation type
as a fraction of ER basin area, (d) tree canopy density, %. In (b) and (c) vegetation type indicated by –
barren (solid black), conifer (solid gray) and aspen (dashed black).

Author Manuscript

This article is protected by copyright. All rights reserved.

Author Manuscript

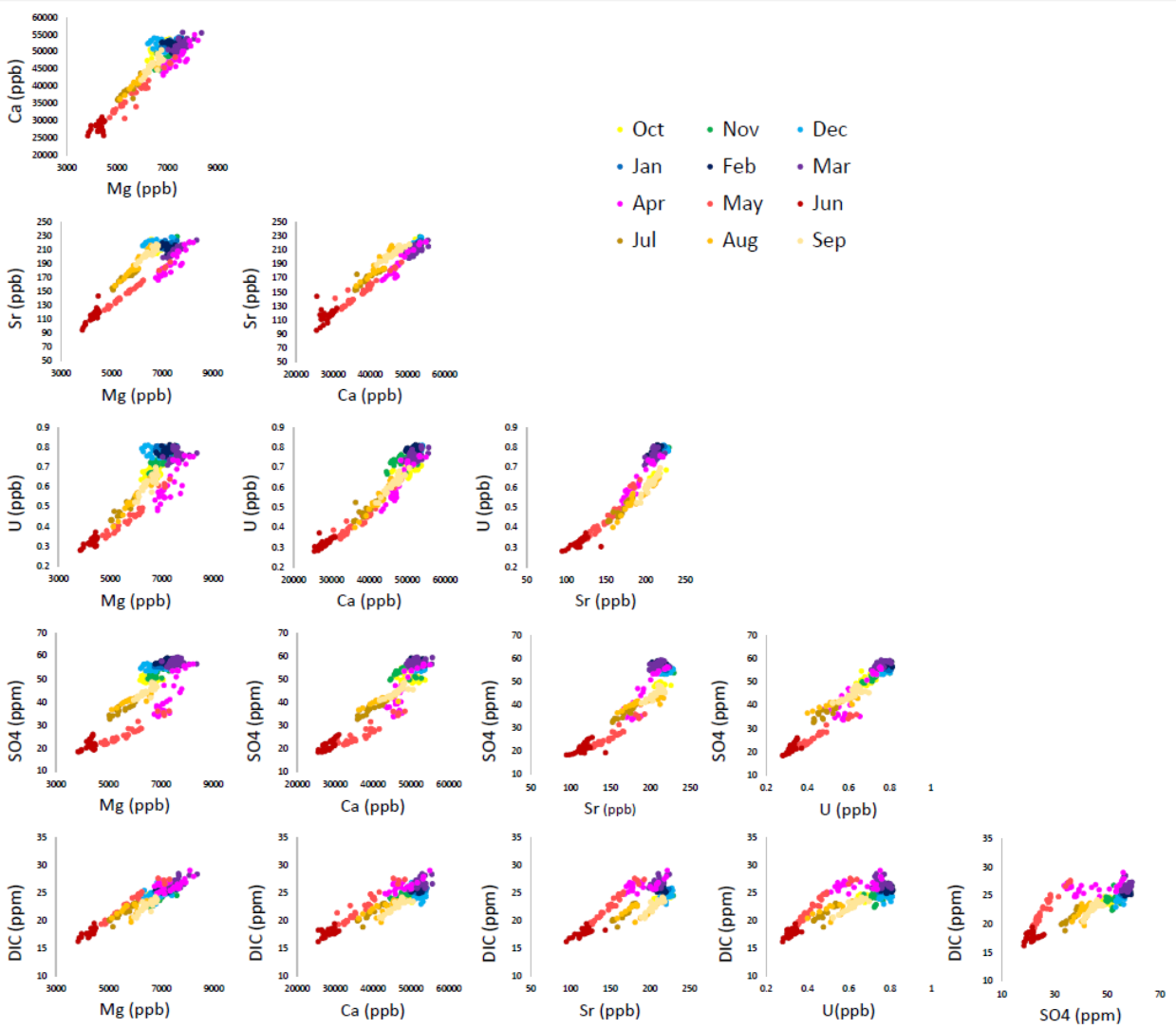


Figure 6. Bi-mixing plots of Pumphouse stream solutes for water year 2016 considered for EMMA.

This article is protected by copyright. All rights reserved.

Author Manuscript

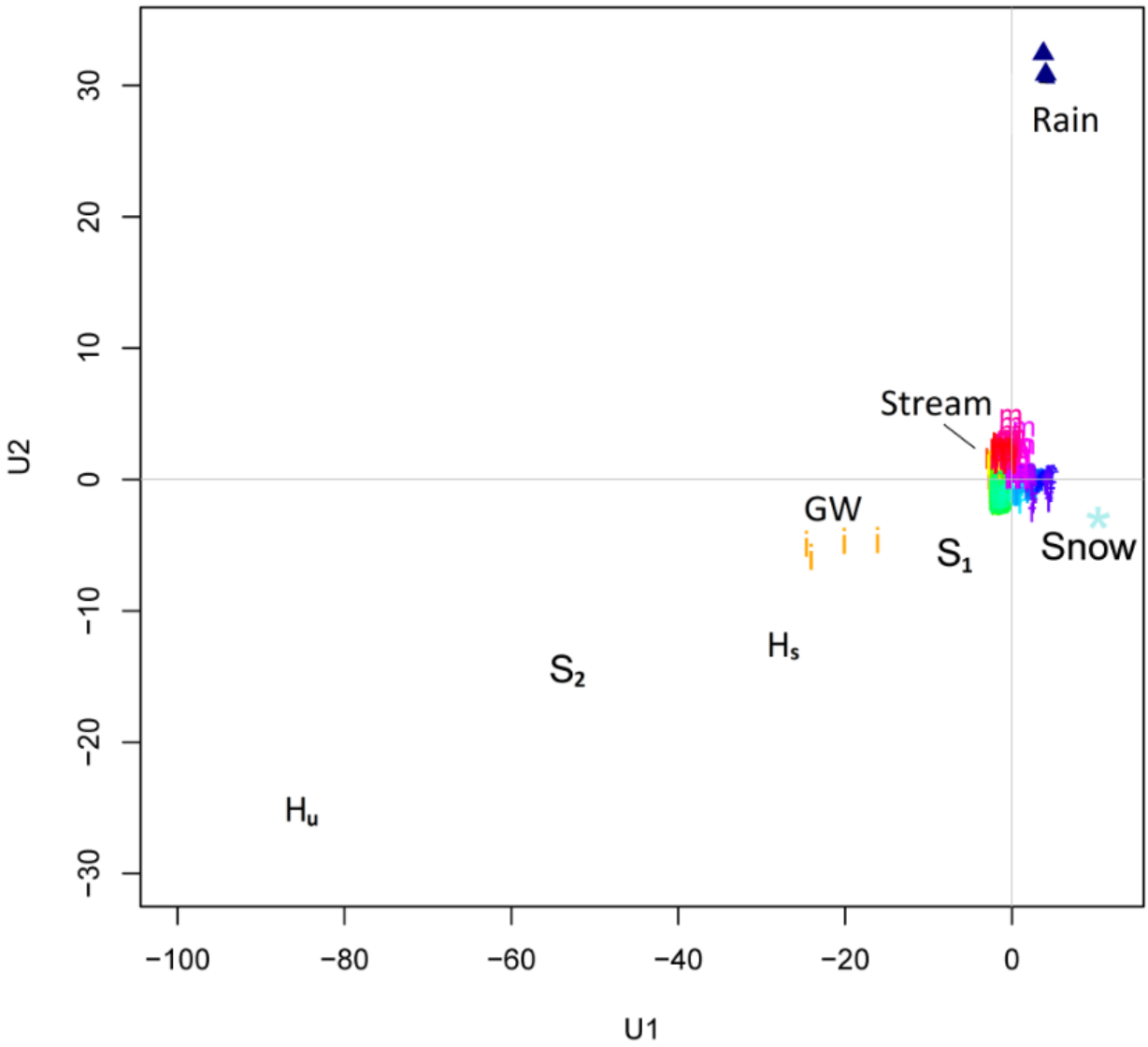


Figure 7. PCA derived U-space positioning of daily Pumphouse streamflow, and end-members defining rain,
snow, and deep groundwater (GW) for hydrographic separation. Seep samples collected in May (S1) and
June (S2), and hillslope well chemistry in November for unsaturated (Hu) and saturated (Hs) conditions are
plotted for comparison and discussed in section 5.2.1.

This article is protected by copyright. All rights reserved.

Author Manuscript

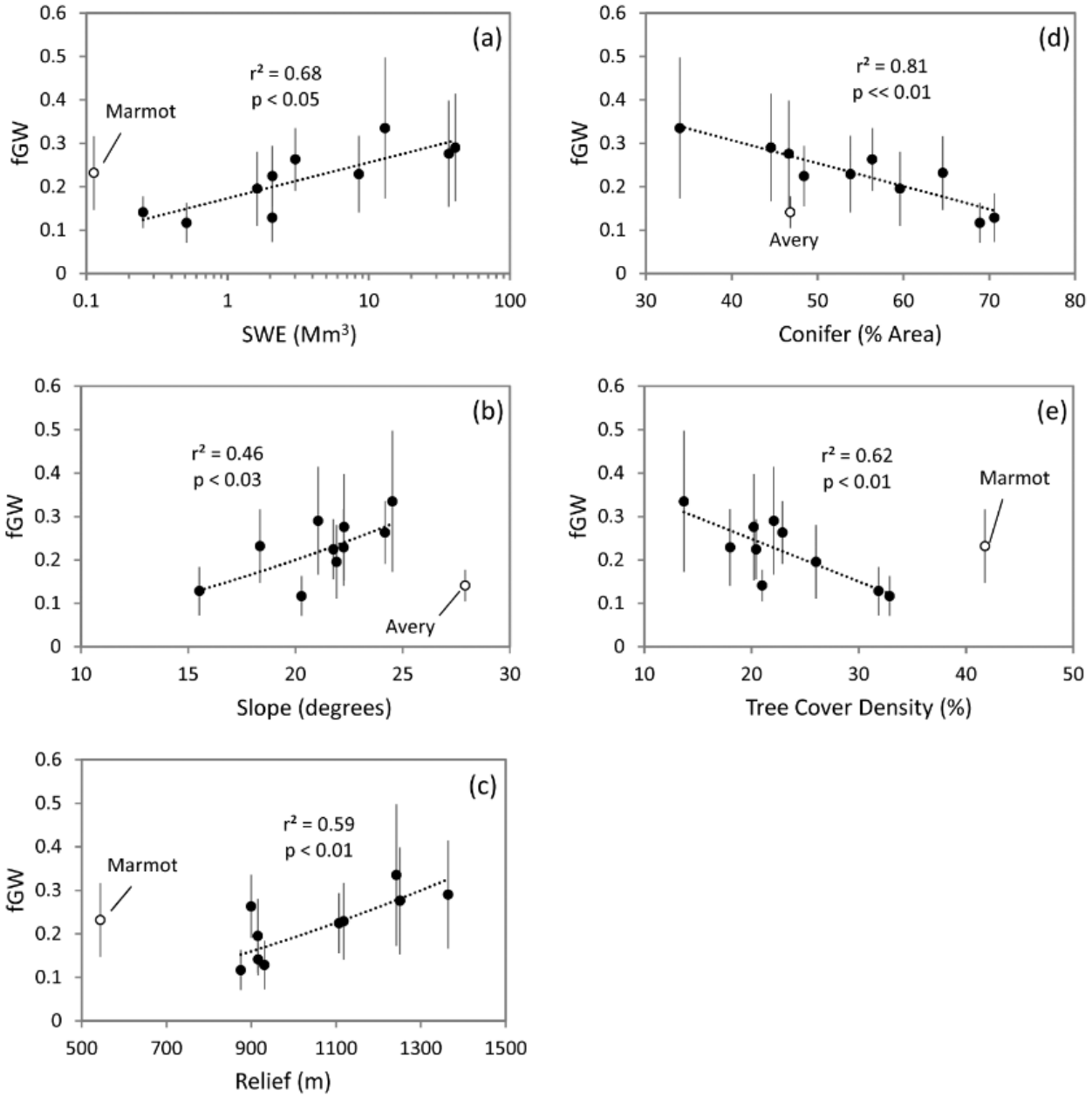


Figure 8. Regressions of basin fraction of streamflow that is groundwater, fGW (annual mean ± range) with
respect to (a) SWE, (b) slope, (c) relief, (d) conifer by area, and (e) tree cover density. Data points
excluded from a regression are shown as a white symbol.

This article is protected by copyright. All rights reserved.

Author Manuscript

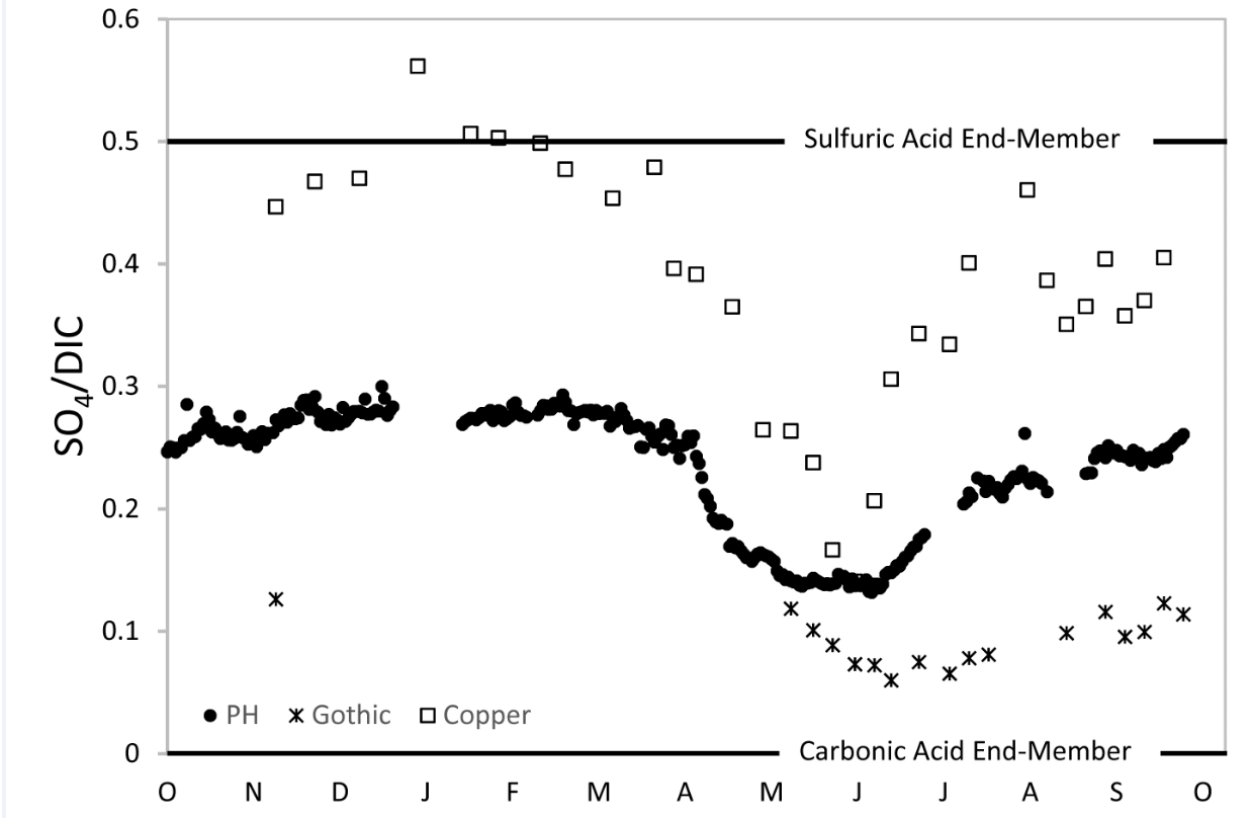


Figure 9. Stream concentration ratios of SO4/DIC for Gothic (ID. 6), Copper (ID. 9) and Pumphouse (ID. 11)
C-Q locations during water year 2016.

This article is protected by copyright. All rights reserved.

Author Manuscript

Figure. 1. ER study site delineated with sampling locations provided. Basin identification numbers provided in Table 1. Stream discharge-concentration sites shown as C-Q, with the Butte and Schofield SNOTEL sites identified by name. Geologic cross section A-A' provided in Figure. 2. (Inset) Location of the ER indicated with a star within the UCRB (black outline) in the context of the western US.

Figure 2. Geologic cross section A-A' traversing the lower floodplain of the ER (Figure 1). Geologic units: Tp and Tg= Oligocene quartz monzonite and granodiorite, respectively; Km = Cretaceous Mancos Formation; Kd = Cretaceous Dakota Sandstone; Jm = Jurassic Morrison Formation; PPm = Permian/Pennsylvanian Maroon Formation; Pg = Pennsylvanian Gothic Formation. Jurassic Entrada Sandstone (Je) not shown but occurs as thin unit at the interface of Jm and PPm. Figure modified from Gaskill et al. (1991).

Figure 3. Water year 2016 snow water equivalent (SWE) at the two SNOTEL sites (Schofield as solid gray and Butte as dashed gray) and daily stream discharge at Pumphouse (solid black). Dates of ASO flight marked (ASO snow depth data presented in section S.1.3).

Figure 4. Spatial distribution of vegetation type. B = Barren/Alpine; C = Conifer; A = Aspen; O = Other; G = Grass; R = Riparian; and S = Shrub.

Figure 5. ER elevational trends in (a) SWE, Mm3, (b) snow depth by vegetation type, m, (c) vegetation type as a fraction of ER basin area, (d) tree canopy density, %. In (b) and (c) vegetation type indicated by – barren (solid black), conifer (solid gray) and aspen (dashed black).

Figure 6. Bi-mixing plots of Pumphouse stream solutes for water year 2016 considered for EMMA.

Figure 7. PCA derived U-space positioning of daily Pumphouse streamflow, and end-members defining rain, snow, and deep groundwater (GW) for hydrographic separation. Seep samples collected in May (S1) and June (S2), and hillslope well chemistry in November for unsaturated (Hu) and saturated (Hs) conditions are plotted for comparison and discussed in section 5.2.1.

Figure 8. Regressions of basin fraction of streamflow that is groundwater, fGW (annual mean ± range) with respect to (a) SWE, (b) slope, (c) relief, (d) conifer by area, and (e) tree cover density. Data points excluded from a regression are shown as a white symbol.

Figure 9. Stream concentration ratios of SO4/DIC for Gothic (ID. 6), Copper (ID. 9) and Pumphouse (ID. 11) C-Q locations during water year 2016.

This article is protected by copyright. All rights reserved.

Author Manuscript

Table 1. ER basin characteristics

Basin ID	name	Area[a]	Elev[b]	Relief[b]	Slope[b]	Aspect[b]	SWE[c]	Mancos[d]	Vegetation Type[e]			Tree Density[f]
									Barren	Conifer	Aspen	
1	EAQ[h]	5.27	3349	900	24	127	3.02	0.70	0.25	0.58	0.04	23
2	Quigley	2.55	3380	915	22	85	1.62	0.62	0.23	0.61	0.01	26
3	Rustlers	14.78	3490	1,118	22	196	8.51	0.08	0.24	0.54	0.00	18
4	Bradley	3.82	3504	1,107	22	242	2.08	0.01	0.41	0.50	0.00	20
5	Rock	3.57	3375	931	16	119	2.07	0.68	0.08	0.72	0.00	32
6	Gothic	0.90	3379	875	20	164	0.51	0.34	0.23	0.70	0.00	33
7	Marmot	0.38	3152	544	18	232	0.11	0.00	0.02	0.87	0.06	42
8	Avery	0.60	3390	916	28	243	0.25	0.00	0.34	0.52	0.02	21
9	Copper	23.67	3528	1,242	25	199	13.02	0.01	0.50	0.36	0.02	14
10	EBC[h]	69.81	3421	1,251	22	182	36.92	0.18	0.32	0.49	0.04	20
11[g]	Pumphouse[h]	84.73	3346	1,364	21	175	41.05	0.18	0.27	0.48	0.09	22

[a]units of km^2

[b]mean values for elevation (m), slope (%) and aspect (degrees); relief (m)

[c]described in section 3.3 (Mm^3)

[d]fraction of basin area mapped at surface

[e]fraction of basin area

[f]area weighted %

[g]EMMA reference cite

[h]occur on main stem of the East River (ER)

This article is protected by copyright. All rights reserved.

Table 2. Water year 2016 flow characteristics of ER basins. Q = average discharge; Q_b = average baseflow; Q_p = peak discharge.

Basin ID	name	Q	Q_b	Q_p		% Pumphouse	
		$m^3 s^{-1}$		$m^3 s^{-1}$	date	Q	Q_b
1	EAQ	0.12	0.02	1.68	10-Jun	7.5	3.6
2	Quigley	0.04	0.02	0.39	10-Jun	2.3	3.9
3	Rustlers	0.35	0.07	4.19	8-Jun	21.5	15.4
4	Bradley	0.06	0.01	0.68	11-Jun	3.5	1.9
5	Rock	0.04	0.01	0.51	5-Jun	2.5	2.5
6	Gothic	0.01	0.0003	0.26	11-Jun	0.6	0.1
7	Marmot	0.01	0.00	0.07	7-Jun	0.5	0.6
8	Avery	0.02	0.01	0.06	21-May	1.2	3.1
9	Copper	0.41	0.11	3.47	10-Jun	25.4	25.0
10	EBC*	1.06	0.26	10.90	10-Jun	65.1	56.0
11	Pumphouse	1.63	0.46	12.20	11-Jun	1.0	1.0

*EBC flows are given as the sum of all measured upstream contributions (1-9)

Author Manuscript

This article is protected by copyright. All rights reserved.

Table 3. Fraction of Pumphouse stream flow source contributions based on three end-members for baseflow (b), rising limb (r), falling limb (f), and monsoon (m) hydrographic periods. GW = deep groundwater.

Period	fGW	fSnow	fRain
b	0.43	0.48	0.09
r	0.22	0.69	0.08
f	0.18	0.74	0.08
m	0.31	0.53	0.16

Author Manuscript

This article is protected by copyright. All rights reserved.

Table 4. Groundwater fractions of streamflow (fGW) for ER sub-basins. Fractions given as mean with uncertainty provided as (minimum – maximum).

Basin	baseflow (b)	rising (r)	falling (f)	monsoon (m)
EAQ	0.37 (0.29-0.50)	0.23 (0.20-0.29)	0.22 (0.18-0.28)	0.32 (0.26-0.41)
Quigley	0.28 (0.22-0.28)	0.11 (0.09-0.14)	0.16 (0.13-0.20)	0.25 (0.20-0.32)
Rustlers	0.33 (0.26-0.45)	0.21 (0.17-0.26)	0.16 (0.13-0.20)	0.26 (0.21-0.34)
Bradley	0.31 (0.25-0.42)	0.21 (0.17-0.26)	0.17 (0.14-0.21)	0.24 (0.19-0.31)
Rock	0.20 (0.16-0.27)	0.09 (0.17-0.11)	0.09 (0.07-0.11)	0.18 (0.14-0.23)
Gothic	0.17 (0.13-0.23)	0.07 (0.06-0.09)	0.07 (0.06-0.09)	0.15 (0.12-0.20)
Marmot	0.34 (0.27-0.46)	0.20 (0.17-0.25)	0.17 (0.14-0.21)	0.28 (0.22-0.36)
Avery	0.21 (0.17-0.29)	0.15 (0.12-0.18)	0.14 (0.12-0.18)	0.18 (0.15-0.23)
Copper	0.50 (0.39-0.68)	0.27 (0.22-0.34)	0.17 (0.14-0.22)	0.32 (0.26-0.41)
EBC	0.41 (0.32-0.55)	0.23 (0.19-0.28)	0.16 (0.14-0.20)	0.29 (0.24-0.38)
Pumphouse	0.43 (0.34-0.58)	0.22 (0.19-0.28)	0.18 (0.15-0.23)	0.31 (0.25-0.40)

Author Manuscript

This article is protected by copyright. All rights reserved.

Table 5. ER upper basin bias calculated using the Pumphouse mixing space.

ID	Basin	Ca	Sr	U	SO_4	δ^2H	$\delta^{18}O$
1	EAQ	-0.21	0.05	0.29	-0.07	0.002	-0.002
2	Quigley	0.01	0.05	0.40	-0.57	0.004	-0.005
3	Rustlers	-0.08	0.15	0.11	-0.23	0.005	-0.001
4	Bradley	-0.18	0.29	0.22	-0.40	0.009	-0.001
5	Rock	0.11	-0.05	0.25	-0.41	-0.003	-0.001
6	Gothic	0.15	-0.09	0.02	-0.13	-0.005	0.001
7	Marmot	-0.27	-0.02	0.40	0.04	0.001	-0.002
8	Avery	0.00	0.18	-0.22	-0.04	0.002	0.004
9	Copper	0.17	0.10	-0.27	-0.13	0.004	0.000
10	EBC	0.01	0.07	-0.01	-0.11	0.001	0.001

Author Manuscript

This article is protected by copyright. All rights reserved.